

J. Plasma Phys. (2022), vol. 88, 905880303 © The Author(s), 2022.Published by Cambridge University Press doi:10.1017/S0022377822000289

# Improved multispecies Dougherty collisions

Manaure Francisquez <sup>10,2</sup>,†, James Juno <sup>03</sup>, Ammar Hakim, Gregory W. Hammett <sup>10</sup> and Darin R. Ernst <sup>10</sup>

<sup>1</sup>Princeton Plasma Physics Laboratory, Princeton, NJ 08543, USA
<sup>2</sup>MIT Plasma Science and Fusion Center, Cambridge, MA 02139, USA
<sup>3</sup>Department of Physics & Astronomy, University of Iowa, Iowa City, IA 52242, USA

(Received 29 December 2021; revised 13 March 2022; accepted 14 March 2022)

The Dougherty model Fokker–Planck operator is extended to describe nonlinear full-*f* (*f* is the distribution function) collisions between multiple species in plasmas. Simple relations for cross-species primitive moments are developed which obey conservation laws, and reproduce familiar velocity and temperature relaxation rates. This treatment of multispecies Dougherty collisions, valid for arbitrary mass ratios, avoids unphysical temperatures and satisfies the *H*-theorem (*H* is related to the entropy) unlike an analogous Bhatnagar–Gross–Krook operator. Formulas for both a Cartesian velocity space and a gyroaveraged operator are provided for use in Vlasov as well as long-wavelength gyrokinetic models. We present an algorithm for the discontinuous Galerkin discretization of this operator, and provide results from relaxation and Landau damping benchmarks.

**Key words:** plasma dynamics, plasma simulation

# 1. Introduction

Collisions play an important role in many laboratory and astrophysical plasma processes of interest. They offer a velocity-space dissipative channel in kinetic turbulence and modify transport in fusion devices, to mention a couple. In continuum kinetic models for plasmas, where small-angle collisions prevail, the effect of collisions is incorporated by the Fokker-Planck operator (FPO) (Rosenbluth, MacDonald & Judd 1957). The gyrokinetic form of this operator also exists (Li & Ernst 2011; Hirvijoki, Brizard & Pfefferlé 2017; Jorge et al. 2019; Pan & Ernst 2019) and has been shown to agree closely with 'model' operators in some parameter ranges (Pan, Ernst & Crandall 2020), but it can also produce significantly different results in others, particularly for instabilities and turbulence driven by the electron temperature gradient (Pan, Ernst & Hatch 2021). Nevertheless, exact FPOs often prove to be analytically and numerically challenging for certain applications. Thus, there is still great interest in using simpler 'model' collision operators, several of which have arisen in the last several years (Abel et al. 2008; Sugama, Watanabe & Nunami 2009; Estève et al. 2015; Sugama et al. 2019; Frei et al. 2021). These model operators compromise accurate physics for tractability of calculations. Yet, these approaches may still have sufficient complexity to deter their use, and mostly exist in

† Email address for correspondence: mfrancis@pppl.gov

linearized form for use in  $\delta f$  studies, f is the distribution function (e.g. Kolesnikov, Wang & Hinton 2010).

The FPO's drag and diffusion terms appear in terms of per unit time increments  $\langle \Delta v_i \rangle_s$  and  $\langle \Delta v_i \Delta v_j \rangle_s$ . A particularly convenient choice is  $\langle \Delta v_i \rangle_s = -\sum_r v_{sr}(v_i - u_{sr,i})$  and  $\langle \Delta v_i \Delta v_j \rangle_s = 2\sum_r v_{sr}v_{t,sr}^2 \delta_{ij}$ ,  $v_{sr}$  being a suitably chosen collision frequency  $(i = \{1, \ldots, d_v\})$  labels the velocity component in  $d_v$ -dimensional velocity space). This approximation leads to the simple model FPO

$$\left(\frac{\mathrm{d}f_s}{\mathrm{d}t}\right)_c = \sum_r \nu_{sr} \nabla_{\mathbf{v}} \cdot \left[ (\mathbf{v} - \mathbf{u}_{sr}) f_s + v_{t,sr}^2 \nabla_{\mathbf{v}} f_s \right]. \tag{1.1}$$

For self-species collisions  $u_{sr} = u_s$  and  $v_{t,sr}^2 = v_{t,s}^2 = T_s/m_s$  are the flow velocity and the squared thermal speed of species s, defined in terms of the velocity moments of the distribution function  $(M_{0,s}, M_{1i,s}, M_{2,s})$  as

$$u_{s,i}M_{0,s} = M_{1i,s}, u_{s,i}M_{1i,s} + d_v v_t^2 M_{0,s} = M_{2,s},$$
(1.2)

with such moments given by

$$M_{0,s} = \int_{-\infty}^{\infty} f_s \, \mathrm{d}^{d_v} v,$$

$$M_{1i,s} = \int_{-\infty}^{\infty} v_i f_s \, \mathrm{d}^{d_v} v,$$

$$M_{2,s} = \int_{-\infty}^{\infty} v^2 f_s \, \mathrm{d}^{d_v} v.$$
(1.3)

This frequently used model goes by the various appellations of the Kirkwood, Lenard–Bernstein or Dougherty operator. We refer to it as the LBO for simplicity. Its nonlinearity is implicit, since the primitive moments  $u_{sr,i}$  and  $v_{t,sr}^2$  are themselves functions of the moments of  $f_{s,r}$ . We also restrict ourselves to the case of velocity independent collisionality; improvements that retain this additional complexity will be explored in the future. The result is then a tractable operator which, owing to its simplicity, conservative properties, and similarity to the full FPO, is used in numerous kinetic plasma models and, with appropriate modifications, virtually every gyrokinetic model.

These attributes also make it an attractive choice for multispecies collisions. Analytic and computational studies have used Dougherty electron–ion collisions for several decades to the present day (Ong & Yu 1970; Pan *et al.* 2018; Shi *et al.* 2019). This trend, however, has not established the most appropriate choice of cross-velocities and thermal speed,  $u_{sr,i}$  and  $v_{t,sr}$ . A study of the universal instability, for example, used  $u_{sr,i} = [m_r n_r/(m_s n_s)]u_{r,i}$  and  $v_{t,sr} = v_{t,s}$ , where  $n_s$  is the number density of species s (Ong & Yu 1970), while a separate analysis of ion-acoustic and drift waves later employed  $u_{sr,i} = [v_{rs}m_r/(v_{sr}m_s)]u_{s,i}$  (Ong & Yu 1973). Dougherty & Watson (1967) had proposed a linearized multispecies version of the eponymous operator with  $u_{sr,i} = u_{r,i}$  and  $v_{t,sr}^2 = [m_r/(m_s + m_r)](v_{t,s}^2 + v_{t,r}^2)$ . More recently Jorge, Ricci & Loureiro (2018) chose  $u_{sr,i} = u_{s,i}$  and  $v_{t,sr} = v_{t,s}$  for exploring drift waves at arbitrary collisionality. Adding to the variance of choices,  $u_{ei} = u_i$  and  $v_{t,ei}^2 = v_{t,e}^2 + (u_i - u_e)^2/3$  were assumed in GENE and Gkeyll full-f gyrokinetic simulations of LArge Plasma Device (LAPD) and National Spherical Torus Experiment (NSTX) (Pan *et al.* 2018; Shi *et al.* 2019). Furthermore, the choice of  $u_{sr}$  and  $v_{t,sr}$  is related to the

adoption of a particular collision frequency  $v_{sr}$ , which Dougherty (1964) and other works left unspecified, although Dougherty & Watson (1967) show one possible choice for the linearized operator.

There has thus been a prolonged, non-systematic spread in the choice of cross-species primitive moments,  $u_{sr,i}$  and  $v_{t,sr}$ , for multispecies collisions with the Dougherty operator. While some of the choices listed above are intuitive and appropriate in some limits, the goal of this manuscript is to more rigorously determine such cross-species primitive moments. Greene (1973), for example, imposed momentum and energy conservation in electron–ion collisions with a Bhatnagar–Gross–Krook (BGK) operator (Bhatnagar, Gross & Krook 1954), and required that the cross-species velocity and temperature relaxation rates match those given by the Boltzmann collision integral for Maxwellian distributions: the Morse relaxation rates (Morse 1963). This procedure yields relations for the  $u_{sr,i}$  and  $v_{t,sr}$  needed by the multispecies BGK model. Unfortunately, for unequal masses the resulting formulas can prescribe a negative  $v_{t,sr}^2$  as the relative drift  $|u_{s,i} - u_{r,i}|$  increases. It has also been pointed out that, although conservative, this multispecies BGK operator cannot be proven to have (or not have) an H-theorem (Haack, Hauck & Murillo 2017).

In what follows we present three different approaches to determining the Dougherty cross-species primitive moments  $u_{sr}$  and  $v_{t,sr}$ , drawing from the ideas of Greene (1973) and Haack et al. (2017) employed for the BGK operator. We begin with the presentation of these approaches in the context of Vlasov-Maxwell models (§ 2). The proposed multispecies full-f nonlinear Dougherty operator is also shown to not decrease the entropy. Entropy production stands as a challenging constraint in some other collision models. For example, a modern linear  $\delta f$  formulation of multispecies collisions only has an H-theorem when temperatures are equal (Sugama et al. 2019). Furthermore, there is little work on full-f collision models; one such operator presented by Estève et al. (2015) has been linearized and is also only able to satisfy the H-theorem for equal temperatures. Section 2 ends with a provision of equivalent formulas for the gyroaveraged Dougherty operator which is frequently used in long-wavelength gyrokinetic simulations (Francisquez et al. 2020). These formulas are then implemented in the discontinuous Galerkin code Gkeyll (2020) using an algorithm described in § 3. Then, § 4 provides a series of Vlasov and gyrokinetic benchmarks illustrating the conservative properties of the algorithm and the differences between the three different strategies for selecting multispecies primitive moments. We also provide a benchmark comparing the Landau damping rate of electron Langmuir waves with the multispecies Dougherty operator against the results using a FPO. Concluding remarks are provided in § 5.

## 2. Multispecies Dougherty operators

In this section we provide three different sets of formulas for the cross-species primitive moments in the LBO. The first is analogous to Greene's treatment of the BGK operator (Greene 1973) and we therefore name it the LBO-G. It introduces a free parameter that is insufficiently constrained at present. We thus complement that approach with the ideas of Haack *et al.* (2017), where two different BGK operators were proposed which independently attempt to match the FPO's momentum and thermal relaxation rates. These are the LBO-EM and LBO-ET, respectively (these operators were also recently implemented in the GENE-X code Ulbl, Michels & Jenko 2021). We conclude this section with similar formulas for a gyroaveraged multispecies Dougherty operator.

## 2.1. *LBO-G*

In the same vein as was done for the BGK in Greene (1973), one may enforce exact momentum and energy conservation, and use Boltzmann relaxation rates (Morse 1963)

to obtain the cross-species primitive moments appropriate for Dougherty electron—ion collisions. Conservation of momentum and energy in cross-species collisions

$$\int_{-\infty}^{\infty} v_i \sum_{s} m_s C[f_s] d^{d_v} v = 0, \qquad (2.1)$$

$$\int_{-\infty}^{\infty} \frac{1}{2} v^2 \sum_{s} m_s C[f_s] d^{d_v} v = 0$$
 (2.2)

 $(C[f_s]$  the right-hand side of (1.1) with  $r \neq s$ ) is obeyed pairwise and yields the relations

$$\sum_{s} m_{s} n_{s} v_{sr} \Delta u_{sr,i} = 0,$$

$$\sum_{s} m_{s} n_{s} v_{sr} \left( d_{v} \Delta v_{t,sr}^{2} + \boldsymbol{u}_{s} \cdot \Delta \boldsymbol{u}_{sr} \right) = 0,$$
(2.3)

with the sum running only over two species (r labels the species other than s),  $\Delta u_{sr} = u_s - u_{sr}$  and  $\Delta v_{t,sr}^2 = v_{t,s}^2 - v_{t,sr}^2$ . This system of  $2(d_v + 1)$  unknowns can be closed in a number of ways; a particularly simple way is by employing the momentum and thermal relaxation rates of the full Coulomb collision operator (see (15) and (16) in Morse 1963). For small-angle collisions these rates are

$$\frac{\partial}{\partial t} m_s n_s u_{s,i} \Big|_{\text{FPO}} = \frac{\alpha_E}{2} \left( m_s + m_r \right) \left( u_{r,i} - u_{s,i} \right),$$

$$\frac{\partial}{\partial t} \frac{d_v}{2} m_s n_s v_{t,s}^2 \Big|_{\text{FPO}} = \frac{\alpha_E}{2} \left[ d_v \left( m_r v_{t,r}^2 - m_s v_{t,s}^2 \right) + m_r \left( \mathbf{u}_r - \mathbf{u}_s \right)^2 \right].$$
(2.4)

The parameter  $\alpha_E$  is inversely proportional to the energy and momentum relaxation times

$$\alpha_E = \frac{2n_s n_r (q_s q_r)^2 \log \Lambda_{sr}}{3(2\pi)^{3/2} \epsilon_0^2 m_s m_r (v_{ts}^2 + v_{tr}^2)^{3/2}}.$$
(2.5)

The right-hand side of (2.4) originates from the Boltzmann collision integral for Coulomb interactions, truncated at the Debye length, under the premise that  $f_s$  are close to Maxwellian. The validity of the relations given below in systems where the plasma may significantly differ from Maxwellian is thus limited.

One can compute the LBO momentum and thermal relaxation rates similar to those for the FPO in (2.4) simply by taking velocity moments of (1.1). These rates are

$$\frac{\partial}{\partial t} m_s n_s u_{s,i} \Big|_{\text{LBO}} = m_s n_s v_{sr} (u_{sr,i} - u_{s,i}),$$

$$\frac{\partial}{\partial t} \frac{d_v}{2} m_s n_s v_{t,s}^2 \Big|_{\text{LBO}} = d_v m_s n_s v_{sr} (v_{t,sr}^2 - v_{t,s}^2).$$
(2.6)

Equating (2.4) and (2.6) does not fully determine  $u_{sr}$  and  $v_{t,sr}^2$  because of the as-of-yet arbitrary  $v_{sr}$ . The next step in the Greene methodology is thus to adopt a relationship between the collision frequency in the model operator and  $\alpha_E$ , which for the BGK operator

<sup>&</sup>lt;sup>1</sup>Dougherty & Watson (1967) have an erroneous extra factor of 3 in the equivalent momentum rate of change, their (2.6).

Greene took to be  $v_{sr} = \alpha_E (m_s + m_r)/[(1 + \beta)n_s m_s]$  with the arbitrary parameter  $\beta > -1$ . For the LBO-G we will instead use

$$v_{sr} = \frac{\alpha_E(m_s + m_r)}{\delta_s(1+\beta)m_sn_s},\tag{2.7}$$

with  $\delta_s = 2m_r n_r v_{rs}/(m_s n_s v_{sr} + m_r n_r v_{rs})$ ; it turns out that  $\delta_s$  and  $\beta$  only appear as  $\delta_s(1+\beta)$  so their independent values do not need to be determined separately. We picked this relationship between  $\alpha_E$  and  $\nu_{sr}$  for three reasons. First, we anticipate potential difficulties guaranteeing positivity of  $v_{t,sr}^2$ , although we will see shortly that such problems do not arise with the Dougherty operator for many systems of interest. Second, the formulation presented here avoids the assumption  $m_s n_s v_{sr} = m_r n_r v_{rs}$  used in earlier work (Greene 1973). Lastly, this definition of  $\nu_{sr}$  produces relations that more easily enforce exact conservation in their discrete form.

Equipped with (2.7) we can equate (2.4) and (2.6), and together with (2.3) a linear system in  $u_{sr,i}$ ,  $v_{t,sr}^2$ ,  $u_{rs,i}$  and  $v_{t,rs}^2$  ensues. The solution of this linear problem is

$$u_{sr,i} = u_{s,i} + \delta_s \frac{1+\beta}{2} \left( u_{r,i} - u_{s,i} \right), \tag{2.8}$$

$$v_{t,sr}^2 = v_{t,s}^2 + \frac{\delta_s}{2} \frac{1+\beta}{1+\frac{m_s}{m_r}} \left[ v_{t,r}^2 - \frac{m_s}{m_r} v_{t,s}^2 + \frac{(\boldsymbol{u}_s - \boldsymbol{u}_r)^2}{d_v} \right].$$
 (2.9)

One attractive property of these cross-species primitive moments is that, contrary to their BGK counterparts, they do not suffer from the pathology of negative  $v_{t,ie}^2$  at supersonic values of the relative drift  $|u_s - u_r|$ . Positivity of (2.9) does require, however, that

$$\frac{\delta_s}{2} \frac{1+\beta}{1+\frac{m_r}{m_s}} \left[ 1 - \frac{T_r}{T_s} - \frac{(\boldsymbol{u}_s - \boldsymbol{u}_r)^2}{d_v c_{s,sr}^2} \right] < 1, \tag{2.10}$$

where  $c_{s,sr} = \sqrt{T_s/m_r}$ . This is true for any choice of  $\delta_s$  and  $\beta$  provided  $\delta_s(1+\beta) < 2$ , even as the relative drift increases.

Despite such improvements on previous similar multispecies operators, the unspecified  $\beta$  parameter poses a clear disadvantage. Dougherty & Watson (1967) had already pointed out that an additional condition is needed to determine all unknowns, and therefore avoid the appearance of any free parameters. As discussed by Haack *et al.* (2017), this free parameter can modify the transport coefficients in the associated fluid models. For the BGK operator, Morse (1964) eliminated the need for  $\beta$  by assuming  $n_s v_{sr} = n_r v_{rs}$  and requiring that the ratio of the relaxation rate for the momentum difference between the two species to that of the temperature difference be the same for both the FPO and the model operator. However, the resulting multispecies BGK operator does not satisfy the *H*-theorem, discouraging us from pursuing that approach. A possible added constraint that may do away with such parameter is the isotropization rate due to interspecies collisions; imposing such condition is, however, beyond the scope of this manuscript.

## 2.2. LBO-EM and LBO-ET

Following the path charted by Haack *et al.* (2017) for the BGK, one could require that  $u_{sr} = u_{rs}$  and  $m_s v_{t,sr}^2 = m_r v_{t,rs}^2$ . Then the momentum conservation constraint in (2.3) results

6

in

$$u_{sr,i} = \frac{m_s n_s \nu_{sr} u_{s,i} + m_r n_r \nu_{rs} u_{r,i}}{m_s n_s \nu_{sr} + m_r n_r \nu_{rs}},$$
(2.11)

while energy conservation assuming  $m_s v_{t,sr}^2 = m_r v_{t,rs}^2$  yields

$$(n_{s}v_{sr} + n_{r}v_{rs}) m_{s}v_{t,sr}^{2} = m_{s}n_{s}v_{sr}v_{t,s}^{2} + m_{r}n_{r}v_{rs}v_{t,r}^{2} + \frac{m_{s}n_{s}v_{sr}m_{r}n_{r}v_{rs}}{m_{s}n_{s}v_{sr} + m_{r}n_{r}v_{rs}} \frac{(u_{s} - u_{r})^{2}}{d_{v}}.$$
(2.12)

The next step demands that the momentum relaxation rates are the same for both the LBO and the FPO. Setting the momentum relaxation rates equal to each other

$$\frac{\partial}{\partial t} \left( m_s n_s u_{s,i} - m_r n_r u_{r,i} \right) \Big|_{\text{FPO}} = \frac{\partial}{\partial t} \left( m_s n_s u_{s,i} - m_r n_r u_{r,i} \right) \Big|_{\text{LBO}},$$

$$\alpha_E \left( m_s + m_r \right) \left( u_{r,i} - u_{s,i} \right) = m_s n_s \nu_{sr} \left( u_{sr,i} - u_{s,i} \right) - m_r n_r \nu_{rs} \left( u_{rs,i} - u_{r,i} \right),$$
(2.13)

and using (2.11) for  $u_{sr}$  one obtains the relationship

$$\alpha_E(m_s + m_r) = \frac{2m_s n_s \nu_{sr} m_r n_r \nu_{rs}}{m_s n_s \nu_{sr} + m_r n_r \nu_{rs}}.$$
(2.14)

On the other hand, equivalence between thermal relaxation rates

$$\frac{\partial}{\partial t} \frac{d_{v}}{2} \left( m_{s} n_{s} v_{t,s}^{2} - m_{r} n_{r} v_{t,r}^{2} \right) \Big|_{\text{FPO}} = \frac{\partial}{\partial t} \frac{d_{v}}{2} \left( m_{s} n_{s} v_{t,s}^{2} - m_{r} n_{r} v_{t,r}^{2} \right) \Big|_{\text{LBO}},$$

$$\alpha_{E} \left[ d_{v} \left( m_{r} v_{t,r}^{2} - m_{s} v_{t,s}^{2} \right) + \frac{m_{r} - m_{s}}{2} \left( \mathbf{u}_{s} - \mathbf{u}_{r} \right)^{2} \right] = d_{v} \left[ m_{s} n_{s} v_{sr} \left( v_{t,sr}^{2} - v_{t,s}^{2} \right) - m_{r} n_{r} v_{rs} \left( v_{t,rs}^{2} - v_{t,r}^{2} \right) \right], \tag{2.15}$$

with the  $v_{t,sr}^2$  from (2.12) implies that

$$\alpha_{E} \left[ m_{r} v_{t,r}^{2} - m_{s} v_{t,s}^{2} + \frac{m_{r} - m_{s}}{2d_{v}} (\boldsymbol{u}_{s} - \boldsymbol{u}_{r})^{2} \right]$$

$$= \frac{2n_{s} v_{sr} n_{r} v_{rs}}{n_{s} v_{sr} + n_{r} v_{rs}} \left( m_{r} v_{t,r}^{2} - m_{s} v_{t,s}^{2} \right) + \frac{n_{s} v_{sr} - n_{r} v_{rs}}{n_{s} v_{sr} + n_{r} v_{rs}} \frac{m_{s} n_{s} v_{sr} m_{r} n_{r} v_{rs}}{m_{s} n_{s} v_{sr} + m_{r} n_{r} v_{rs}} \frac{(\boldsymbol{u}_{s} - \boldsymbol{u}_{r})^{2}}{d_{v}}. \quad (2.16)$$

Although they may look strongly nonlinear, one can solve (2.14) and (2.16) in order to obtain an expression for  $v_{sr}$ . The result is

$$v_{sr} = \frac{\alpha_E (m_s + m_r)}{n_s m_s} \cdot \frac{\frac{m_s - m_r}{2m_s m_r} d_v \left( m_r v_{t,r}^2 - m_s v_{t,s}^2 \right) + (\boldsymbol{u}_s - \boldsymbol{u}_r)^2}{\frac{1}{m_r} d_v \left( m_r v_{t,r}^2 - m_s v_{t,s}^2 \right) + (\boldsymbol{u}_s - \boldsymbol{u}_r)^2},$$
 (2.17)

but we can immediately notice that this can lead to negative collision frequencies in some parameter regimes; for example, the electron–ionfrequency  $v_{ei}$  with zero relative drift.

<sup>&</sup>lt;sup>2</sup>Haack *et al.* (2017) state that the equivalent equations for the BGK operator are nonlinear and without a simple formula for a solution. But one can obtain such solution by casting (2.14) in terms of  $\tau_{rs} = 1/\nu_{rs}$ , solving for  $\tau_{rs}$  and substituting that into (56) of Haack *et al.* (2017) (the equivalent of our (2.16)). The result is a quadratic equation for  $n_s \nu_{sr}$ , which can be solved.

This indicates that enforcing the equality of momentum and thermal relaxation rates while using the assumptions  $u_{sr,i} = u_{rs,i}$  and  $m_s v_{t,sr}^2 = m_r v_{t,rs}^2$  leads to unphysical behaviour. We nevertheless present two slight variations in the following subsections, as was also recently done by Ulbl *et al.* (2021), in order to provide a point of reference for the LBO-G and comparing against Haack *et al.* (2017).

## 2.2.1. LBO-EM

Instead of trying to match both the momentum and thermal relaxation rates, we could satisfy ourselves with only attaining the same momentum relaxation rate. We can do this by employing (2.14), which we obtained from setting LBO and FPO momentum relaxation rates equal to each other, and further assuming that

$$m_s n_s \nu_{sr} = m_r n_r \nu_{rs}. \tag{2.18}$$

These two equations together set the collision frequency in our model to

$$\nu_{sr}^{M} = \alpha_{E} \frac{m_{s} + m_{r}}{m_{s} n_{s}} = \frac{2 (m_{s} + m_{r}) (q_{s} q_{r})^{2} n_{r} \log \Lambda_{sr}}{3 (2\pi)^{3/2} \epsilon_{0}^{2} m_{s}^{2} m_{r} (v_{ts}^{2} + v_{tr}^{2})^{3/2}}.$$
 (2.19)

This choice of collision frequency reduces the cross-primitive moments to

$$u_{sr,i} = \frac{u_{s,i} + u_{r,i}}{2},$$

$$v_{t,sr}^2 = \frac{1}{1 + \frac{m_s}{m_r}} \left[ v_{t,s}^2 + v_{t,r}^2 + \frac{(u_s - u_r)^2}{2d_v} \right].$$
(2.20)

We call (1.1) with collision frequency and cross-primitive moments in (2.19)–(2.20) the LBO-EM. Compared with the equations that led to LBO-G, (2.19) suggests that LBO-EM is LBO-G in the limit of  $\beta = 0$  and  $\delta_s = 1$ . In this case the cross-species flow velocity in LBO-G (2.8) does reduce to that in LBO-EM, but the LBO-G cross-species thermal velocity in this limit does not equal that in (2.20). Interestingly, for vanishing relative drifts,  $\beta = 1$  leads to an agreement between  $v_{t,sr}^2$  for LBO-G and LBO-EM, but leads to  $u_{sr,i} = u_{r,i}$ , which disagrees with LBO-EM's  $u_{sr,i}$ . Therefore, as with BGK, LBO-EM is not a special case of LBO-G.

## 2.2.2. *LBO-ET*

Alternatively, we could choose to approximately match the thermal relaxation rate of the FPO. Focusing on the temperature difference term in (2.4), we see that the relaxation rate due to temperature differences alone is the same for both species. We could choose to mimic this behaviour, and examining (2.6) the conclusion would be that we have to require

$$n_s \nu_{sr} = n_r \nu_{rs}. \tag{2.21}$$

This assumption renders (2.11)–(2.12) into

$$u_{sr,i} = \frac{m_s u_{s,i} + m_r u_{r,i}}{m_s + m_r},$$
 (2.22)

$$v_{t,sr}^2 = \frac{1}{2} \left[ v_{t,s}^2 + \frac{m_r}{m_s} v_{t,r}^2 + \frac{m_r}{m_s + m_r} \frac{(u_s - u_r)^2}{d_v} \right].$$
 (2.23)

Although we took up relation (2.21) we have not specified the collision frequency precisely yet. We can do so by returning to the thermal relaxation rate equivalence (2.15)

and inserting the cross-species temperature in (2.23). The result is<sup>3</sup>

$$\alpha_{E} \left[ d_{v} \left( m_{r} v_{t,r}^{2} - m_{s} v_{t,s}^{2} \right) + \frac{m_{r} - m_{s}}{2} \left( u_{s} - u_{r} \right)^{2} \right]$$

$$= d_{v} \left[ \frac{n_{s} v_{sr}}{2} \left( m_{r} v_{t,r}^{2} - m_{s} v_{t,s}^{2} + \frac{m_{s} m_{r}}{m_{s} + m_{r}} \frac{(u_{s} - u_{r})^{2}}{d_{v}} \right) \right]$$

$$- \frac{n_{r} v_{rs}}{2} \left( m_{s} v_{t,s}^{2} - m_{r} v_{t,r}^{2} + \frac{m_{s} m_{r}}{m_{s} + m_{r}} \frac{(u_{s} - u_{r})^{2}}{d_{v}} \right) \right], \qquad (2.24)$$

$$\alpha_{E} \left[ \left( m_{r} v_{t,r}^{2} - m_{s} v_{t,s}^{2} \right) + \frac{m_{r} - m_{s}}{2} \frac{(u_{s} - u_{r})^{2}}{d_{v}} \right]$$

$$= \frac{n_{s} v_{sr} + n_{r} v_{rs}}{2} \left( m_{r} v_{t,r}^{2} - m_{s} v_{t,s}^{2} \right) + \frac{1}{2} \frac{m_{s} m_{r}}{m_{s} + m_{r}} \left( n_{s} v_{sr} - n_{r} v_{rs} \right) \frac{(u_{s} - u_{r})^{2}}{d_{v}}.$$

These thermal relaxation rates cannot agree exactly because, under the assumption  $n_s v_{sr} =$  $n_r v_{rs}$ , the relative drift term vanishes for this LBO, but we could at least match the response due to the temperature difference, leading to the collision frequency for this model

$$v_{sr}^{T} = \frac{\alpha_E}{n_s} = \frac{2n_r(q_s q_r)^2 \log \Lambda_{sr}}{3(2\pi)^{3/2} \epsilon_0^2 m_s m_r \left(v_{t,s}^2 + v_{t,r}^2\right)^{3/2}}.$$
 (2.25)

The operator (1.1) with this collision frequency and the cross-primitive moments in (2.22)–(2.23) is referred to as the LBO-ET. As with the previous operator, setting  $\beta = 0$ in the LBO-G leads to the same cross-species flow velocity  $u_{sr,i}$ , but then the thermal speeds  $v_{t,sr}$  do not agree. More importantly, we restate that the LBO-ET did not exactly match the FPO thermal relaxation rate because of the difference in response to relative drifts. For plasmas where the relative drifts are small relative to temperature differences (not an uncommon situation), these rates agree exactly.

#### 2.3. The H-theorem

The full FPO does not decrease entropy, i.e. it satisfies an H-theorem, and as a model FPO it is desirable that this formulation of multispecies Dougherty collisions retains such a property. The original paper on the multispecies Dougherty operator demonstrated a non-decreasing entropy only to second order after linearization (Dougherty & Watson 1967), hinting at the possibility that the above full-f equivalent operator could possess an H-theorem. It is in fact possible, however, to show that the Dougherty models for multispecies full-f collisions presented here do have an H-theorem, even for species with unequal temperatures. A more detailed proof of this statement is given in Appendix B, and we give an outline of the argument here. The total entropy  $S = -\sum_{s} \int d^{d_{v}} v f_{s} \ln f_{s}$  can be shown to obey

$$\dot{S} = \frac{\partial S}{\partial t} = -\sum_{s} \int d^{d_{v}} v \, \nu_{sr} \left( \ln f_{s} + 1 \right) \nabla_{v} \cdot J_{sr}, \tag{2.26}$$

where the flux  $J_{sr}$  is the term in square brackets in (1.1). Using the definition of this flux and integration by parts twice together with the fact that  $f_s \to 0$  faster than powers of  $v_i$  as

<sup>&</sup>lt;sup>3</sup>We believe there is a typo in similar equations for BGK in Haack et al. (2017). In (65) of that paper the relative drift term should be multiplied by  $(m_i + 3m_i)/(2m_i)$ .

 $v_i \to \pm \infty$  one is led to

$$\dot{S} = \sum_{s} \nu_{sr} \left( -d_{v} n_{s} + v_{t,sr}^{2} \int d^{d_{v}} v \, \nabla_{v} f_{s} \cdot \nabla_{v} \ln f_{s} \right). \tag{2.27}$$

At this point we can perform a variational minimization of this functional in order to determine if that minimum is below zero (indicating a violation of thermodynamic law). For a given set of primitive moments  $(n_s, u_{s,i}, v_{t,s}, u_{sr,i}, v_{t,sr})$  and the virtual displacement  $\delta f_s = f_s - f_{s0}$ , the response of  $\dot{S}$  is

$$\delta \dot{\mathcal{S}} = \sum_{s} v_{t,sr}^2 \int d^{d_v} v \, \nabla_v f_{s0} \cdot \left[ \frac{2}{\delta f_s} \nabla_v \delta f_s - \frac{1}{f_{s0}} \nabla_v f_{s0} \right] \frac{\delta f_s}{f_{s0}}. \tag{2.28}$$

At an extremum in  $\dot{S}$  this function must vanish, and since (2.27) has no upper bound this extremum must be a minimum. We are also interested in virtual displacements that do not alter the moments of each distribution, that is

$$\int d^{d_v} v \, v^k \delta f_s = 0 \quad \text{for } k \in \{0, 1, 2\}.$$
 (2.29)

Further imposing that the displacement  $\delta f_s$  vanishes at infinity,  $\delta \dot{S} = 0$  and (2.28)–(2.29) yield the nonlinear inhomogeneous equation for the minimizing distribution  $f_{s0}$ 

$$|\nabla_{\mathbf{v}} \ln f_{s0}|^2 + 2\nabla_{\mathbf{v}}^2 \ln f_{s0} = h_0^2 + 2d_{\mathbf{v}}h_1 + 2h_0\mathbf{h}_1 \cdot \mathbf{v} + h_1^2 v^2, \tag{2.30}$$

with  $h_0$ ,  $h_1$  and  $h_2$  undetermined linear coefficients. The solution to this equation is  $f_{s0} \propto \exp(h_{0,i}v_i + h_1v^2/2)$ . Enforcing the condition that it has the same number density  $n_s$  and primitive moments  $(u_{s,i}$  and  $v_{t,s})$  as the original distribution,  $f_s$ , reveals that the distribution that minimizes the rate of entropy change of this operator is a Maxwellian with  $n_s$ ,  $u_{s,i}$  and  $v_{t,s}$ . The final step is to insert this distribution back into our expression for entropy change, (2.26), and check that the minimum entropy rate of change does not fall below zero. Such a procedure results in

$$\min\left(\frac{\partial S}{\partial t}\right) = d_v \sum_{s} \frac{n_s \nu_{sr}}{\nu_{t,s}^2} \left(v_{t,sr}^2 - v_{t,s}^2\right),\tag{2.31}$$

and since the procedure obtained a single minimum it must be the global minimum.

## 2.3.1. LBO-G H-theorem

Use the definition of  $v_{t,sr}^2$  for the LBO-G model (2.9) to arrive at

$$\min\left(\frac{\partial \mathcal{S}}{\partial t}\right) = \frac{\delta_s m_s n_s v_{sr}}{2v_{t,s}^2} \frac{1+\beta}{m_s + m_r} \left[ d_v \frac{(T_r - T_s)^2}{T_s T_r} + \left(\frac{m_r}{m_s} \frac{1}{v_{t,s}^2} + \frac{m_s}{m_r} \frac{1}{v_{t,r}^2}\right) (\boldsymbol{u}_s - \boldsymbol{u}_r)^2 \right] \geqslant 0.$$
(2.32)

We are thus led to the conclusion that the LBO-G model of full-f multispecies collisions does not decrease the entropy. This is in contrast to the BGK-G operator, for which the H-theorem could not be proven or disproven (Greene 1973; Haack *et al.* 2017).

# 2.3.2. LBO-EM and LBO-ET H-theorem

Using the relationship between collision frequencies for the LBO-EM (2.19) and the corresponding cross-species thermal speeds one obtains

$$\min\left(\frac{\partial \mathcal{S}}{\partial t}\right) = \frac{d_v n_s v_{sr}}{m_s + m_r} \left[ \frac{\left(m_r v_{t,r}^2 - m_s v_{t,s}^2\right)^2}{v_{t,s}^2 m_r v_{t,r}^2} + \left(\frac{m_r}{v_{t,s}^2} + \frac{m_s}{m_r} \frac{m_s + m_r}{v_{t,r}^2}\right) \frac{(\boldsymbol{u}_s - \boldsymbol{u}_r)^2}{2d_v} \right] \geqslant 0.$$
(2.33)

Similarly, using the  $n_s v_{sr} = n_r v_{rs}$  assumption of the LBO-ET model and the definition of  $v_{tsr}^2$  in (2.23) turns (2.31) into

$$\min\left(\frac{\partial \mathcal{S}}{\partial t}\right) = \frac{d_v n_s v_{sr}}{2} \left[ \frac{m_r v_{t,r}^2}{m_s v_{t,s}^2} + \frac{m_s v_{t,s}^2}{m_r v_{t,r}^2} + \left(\frac{m_r}{v_{t,s}^2} + \frac{m_s}{v_{t,r}^2}\right) \frac{1}{m_s + m_r} \frac{(\boldsymbol{u}_s - \boldsymbol{u}_r)^2}{d_v} \right] \geqslant 0.$$
(2.34)

Therefore, both LBO-EM and LBO-ET models satisfy the *H*-theorem.

# 2.4. Gyroaveraged multispecies Dougherty operator

This model operator is also used by modern, long-wavelength full-f gyrokinetic codes (Pan *et al.* 2018; Gkeyll 2020) in its gyroaveraged form. Its form, conservative properties and discontinuous Galerkin discretization for self-species collisions have been presented by Francisquez *et al.* (2020). The operator can, however, be extended to incorporate cross-species collisions. For that purpose, we write the gyroaveraged operator acting on the guiding centre distribution function  $f_s(R, v_{\parallel}, \mu)$  as

$$\left(\frac{\partial \mathcal{J}f_{s}}{\partial t}\right)_{c} = \sum_{r} \nu_{sr} \left\{ \frac{\partial}{\partial \nu_{\parallel}} \left[ \left( \nu_{\parallel} - u_{\parallel sr} \right) \mathcal{J}f_{s} + \nu_{t,sr}^{2} \frac{\partial \mathcal{J}f_{s}}{\partial \nu_{\parallel}} \right] + \frac{\partial}{\partial \mu} 2\mu \left[ \mathcal{J}f_{s} + \frac{m_{s}\nu_{t,sr}^{2}}{B} \frac{\partial \mathcal{J}f_{s}}{\partial \mu} \right] \right\},$$
(2.35)

where  $\mathcal{J}$  represents the Jacobian of the guiding centre coordinates,  $\mathbf{R}$  is the guiding centre position,  $v_{\parallel}$  is the velocity along the background magnetic field and  $\mu$  is the adiabatic moment; see Francisquez *et al.* (2020) for more details.

In order to use this multispecies gyroaveraged operator one must then determine the multispecies parallel flow velocities  $u_{\parallel sr}$  and thermal speed  $v_{t,sr}$ . Our proposal is to use the same LBO-G (2.8), (2.9), LBO-EM (2.20) and LBO-ET (2.22)–(2.23) models with this gyroaveraged operator. The only difference is that the self-species primitive moments are defined by

$$u_{\parallel s} M_{0,s} = M_{1,s},$$
  

$$u_{\parallel s} M_{1,s} + d_v v_{t,s}^2 M_{0,s} = M_{2,s},$$
(2.36)

where  $d_v = 1$  or  $d_v = 3$  depending on whether one is considering  $v_{\parallel}$ - or  $(v_{\parallel}, \mu)$ -space, respectively. The velocity moments in the gyroaveraged model are

$$M_{0,s} = (2\pi/m_s) \int \mathcal{J}f_s(\mathbf{R}, v_{\parallel}, \mu) \, \mathrm{d}v_{\parallel} \, \mathrm{d}\mu,$$

$$M_{1\parallel,s} = (2\pi/m_s) \int v_{\parallel} \mathcal{J}f_s(\mathbf{R}, v_{\parallel}, \mu) \, \mathrm{d}v_{\parallel} \, \mathrm{d}\mu,$$

$$M_{2,s} = (2\pi/m_s) \int \left(v_{\parallel}^2 + 2\mu B/m_s\right) \mathcal{J}f_s(\mathbf{R}, v_{\parallel}, \mu) \, \mathrm{d}v_{\parallel} \, \mathrm{d}\mu.$$

$$(2.37)$$

## 3. Discontinuous Galerkin discretization

In this section we present a discontinuous Galerkin (DG) scheme for the multispecies LBO. DG algorithms offer higher-orderconvergence, data locality and flexibility in defining numerical fluxes to preserve physical properties of the system (Cockburn & Shu 1998; Hesthaven & Warburton 2007). A DG discretization will also interface with existing Vlasov–Maxwell (Juno *et al.* 2018; Hakim & Juno 2020) and gyrokinetic (Shi *et al.* 2019; Mandell *et al.* 2020) DG solvers.

We present the algorithm below for a two-dimensional space consisting of one position dimension (x) and one velocity dimension (v); the extension to higher velocity dimensions is straightforward. First, introduce a mesh  $\mathcal{T}$  that extends over the finite computational domain  $\Omega \equiv [-L_x/2, L_x/2] \times [-L_v/2, L_v/2]$  and consists of quadrilateral cells  $K_{j,k} \equiv [x_{j-1/2}, x_{j+1/2}] \times [v_{k-1/2}, v_{k+1/2}]$ , with  $j = 1, \ldots, N_x$  and  $k = 1, \ldots, N_v$  labelling the cell along x and v, respectively. In each cell define a polynomial space  $\mathcal{V}_{j,k}^p$  consisting of  $N_b$  orthonormalized monomials  $\psi_\ell(x, v)$ , which we take as basis functions in which dynamical fields are expanded. The discretization of (1.1) proceeds from a weak or Galerkin projection; multiply (1.1) by  $\psi_\ell$  and integrate over x-v in cell  $K_{j,k}$ 

$$\int_{K_{j,k}} \psi_{\ell} \left( \frac{\mathrm{d}f_{s}}{\mathrm{d}t} \right)_{c} \mathrm{d}x \, \mathrm{d}v = \int_{x_{j-1/2}}^{x_{j+1/2}} \nu_{sr} \left( \psi_{\ell} G_{s} - \frac{\partial \psi_{\ell}}{\partial v} v_{t,sr}^{2} \hat{f}_{s} \right) \Big|_{v_{k-1/2}}^{v_{k+1/2}} \mathrm{d}x 
- \int_{K_{j,k}} \nu_{sr} \left[ \frac{\partial \psi_{\ell}}{\partial v} \left( v - u_{sr} \right) f_{s} - \frac{\partial^{2} \psi_{\ell}}{\partial v^{2}} v_{t,sr}^{2} f_{s} \right] \mathrm{d}x \, \mathrm{d}v.$$
(3.1)

We used integration by parts and limited ourselves to the case of two species cross-collisions only to remove the sum in (1.1). The numerical flux  $G_s = (v - u_{sr})f_s + v_{t,sr}^2 \partial \hat{f}_s / \partial v$  consists of a drag term that is computed using upwinding based on the value of the  $(v - u_{sr})$  at Gauss-Legendre nodes, and  $\hat{f}_s$  is a continuous distribution recovered across two cells (van Leer & Nomura 2005; van Leer & Lo 2007). This approach resulted in a conservative DG scheme in the case of self-species collisions; more details can be found in Hakim *et al.* (2020) and Francisquez *et al.* (2020). In the case of multispecies collisions it can also lead to a conservative scheme, provided the cross-species primitive moments are computed in a manner that incorporates the finite extent of velocity space.

In what follows we will also need the velocity moments of each species (1.3) in their discrete form. Discrete moments are defined as expansions in a set of  $N_b^x$  position-space polynomial basis functions  $\varphi_{\ell}(x)$  belonging to the polynomial space  $\mathcal{V}_k^p$  in the *j*th cell. The discrete velocity moments are then projections of (1.3) onto the  $\varphi_{\ell}$  basis, which for  $d_v = 1$ 

we represent as

$$M_{q,s} \doteq \int_{v_{\min}}^{v_{\max}} v^q f_s \, \mathrm{d}v, \quad q \in \{0, 1, 2\},$$
 (3.2)

where  $v_{\min} = v_{k_{\min}-1/2} = v_{1/2}$ ,  $v_{\max} = v_{k_{\max}+1/2} = v_{N_v+1/2}$  and  $\doteq$  indicates weak equality (Francisquez *et al.* 2020; Hakim *et al.* 2020). Two fields g and h are weakly equal in the interval  $I = [x_{j-1/2}, x_{j+1/2}]$  if their projections onto the basis functions in this interval are equal:  $g \doteq h \Rightarrow \int_I (g - h) \varphi_\ell \, dx = 0$ .

# 3.1. Discrete momentum conservation

In order to formulate a momentum-conserving discretization based on (3.1), we can set  $\psi_{\ell} = m_s v$  and sum over all cells along velocity space. According to (2.1) this sum has to be equal and opposite to that of the other species it is colliding with. Therefore discrete momentum conservation requires that

$$\sum_{k} \int_{x_{j-1/2}}^{x_{j+1/2}} \left( m_{s} \nu_{sr} \left\{ \left( vG_{s} - v_{t,sr}^{2} \hat{f}_{s} \right)_{v_{k-1/2}}^{v_{k+1/2}} - \int_{v_{k-1/2}}^{v_{k+1/2}} \left( v - u_{sr} \right) f_{s} \, \mathrm{d}v \right\} \right. \\
+ m_{r} \nu_{rs} \left\{ \left( vG_{r} - v_{t,rs}^{2} \hat{f}_{r} \right)_{v_{k-1/2}}^{v_{k+1/2}} - \int_{v_{k-1/2}}^{v_{k+1/2}} \left( v - u_{rs} \right) f_{r} \, \mathrm{d}v \right\} \right) \mathrm{d}x = 0.$$
(3.3)

Carry out the velocity-space integrals and sum over all velocity-space cells. Use the fact that the numerical fluxes  $G_s$  are continuous and have opposite signs on either side of a cell boundary, and that  $\hat{f}_s$  is continuous across cell boundaries as well. Furthermore, we impose the zero-flux boundary conditions  $G_s(v = v_{\text{max}}) = G_s(v = v_{\text{min}}) = 0$  in order to arrive at

$$\int_{x_{j-1/2}}^{x_{j+1/2}} \left[ m_s v_{sr} \left( v_{t,sr}^2 f_s \Big|_{v_{\min}}^{v_{\max}} + M_{1,s} - u_{sr} M_{0,s} \right) + m_r v_{rs} \left( v_{t,rs}^2 f_r \Big|_{v_{\min}}^{v_{\max}} + M_{1,r} - u_{rs} M_{0,r} \right) \right] dx = 0,$$
(3.4)

having substituted the discrete form of the velocity moments (3.2). This relation is satisfied if

$$m_s v_{sr} \left( v_{t,sr}^2 f_s \Big|_{v_{\min}}^{v_{\max}} + M_{1,s} - u_{sr} M_{0,s} \right) + m_r v_{rs} \left( v_{t,rs}^2 f_r \Big|_{v_{\min}}^{v_{\max}} + M_{1,r} - u_{rs} M_{0,r} \right) \doteq 0. \quad (3.5)$$

Note that we have used the same  $v_{\text{max}}$  and  $v_{\text{min}}$  for both species for pedagogical reasons only. In fact since (3.5) is a constraint on position-space fields only, the discrete velocity space of each species can be completely different. For completeness we state that in the  $d_v$ -dimensional case the condition for the scheme in (3.1) to conserve momentum is that the cross-species primitive moments  $u_{sr}$  and  $v_{t,sr}$  must satisfy

$$m_{s} \nu_{sr} \left( M_{1i,s} - u_{sr,i} M_{0,s} + \nu_{t,sr}^{2} \int f_{s} \Big|_{\nu_{i,\min}}^{\nu_{i,\max}} dS_{i} \right)$$

$$+ m_{r} \nu_{rs} \left( M_{1i,r} - u_{rs,i} M_{0,r} + \nu_{t,rs}^{2} \int f_{r} \Big|_{\nu_{i,\min}}^{\nu_{i,\max}} dS_{i} \right) \doteq 0,$$
(3.6)

using  $\int dS_i$  as an integral over the velocity-space boundaries orthogonal to the *i*th velocity dimension, and the repeated index *i* implies summation.

# 3.2. Discrete energy conservation

Energy conservation will impose a secondary constraint on how the discrete cross-species primitive moments must be computed. In order to obtain such condition we substitute  $\psi_{\ell} = m_s v^2/2$  in (3.1), and sum over velocity-space cells and species. This action leads to

$$\sum_{k} \int_{x_{j-1/2}}^{x_{j+1/2}} \left( m_{s} v_{sr} \left\{ \left( \frac{v^{2}}{2} G_{s} - v v_{t,sr}^{2} \hat{f}_{s} \right) \Big|_{v_{k-1/2}}^{v_{k+1/2}} - \int_{v_{k-1/2}}^{v_{k+1/2}} \left[ v \left( v - u_{sr} \right) f_{s} - v_{t,sr}^{2} f_{s} \right] dv \right\} 
+ m_{r} v_{rs} \left\{ \left( \frac{v^{2}}{2} G_{r} - v v_{t,rs}^{2} \hat{f}_{r} \right) \Big|_{v_{k-1/2}}^{v_{k+1/2}} - \int_{v_{k-1/2}}^{v_{k+1/2}} \left[ v \left( v - u_{rs} \right) f_{r} - v_{t,rs}^{2} f_{r} \right] dv \right\} \right) dx = 0.$$
(3.7)

Once again, we employ continuity of  $G_s$  and  $\hat{f}_s$  and boundary conditions so that after performing the velocity-space integrals and carrying out the sum over velocity-space cells this relation is transformed into

$$\int_{x_{j-1/2}}^{x_{j+1/2}} \left( m_s v_{sr} \left\{ v v_{t,sr}^2 f_s \Big|_{v_{\min}}^{v_{\max}} + \left( M_{2,s} - u_{sr} M_{1,s} \right) - v_{t,sr}^2 M_{0,s} \right\} + m_r v_{rs} \left\{ v v_{t,rs}^2 f_r \Big|_{v_{\min}}^{v_{\max}} + \left( M_{2,r} - u_{rs} M_{1,r} \right) - v_{t,rs}^2 M_{0,r} \right\} \right) dx = 0.$$
(3.8)

Therefore, we can guarantee that our DG discretization exactly conserves energy if we enforce

$$m_{s}v_{sr}\left\{vv_{t,sr}^{2}f_{s}\Big|_{v_{\min}}^{v_{\max}}+\left(M_{2,s}-u_{sr}M_{1,s}\right)-v_{t,sr}^{2}M_{0,s}\right\} + m_{r}v_{rs}\left\{vv_{t,rs}^{2}f_{r}\Big|_{v_{\min}}^{v_{\max}}+\left(M_{2,r}-u_{rs}M_{1,r}\right)-v_{t,rs}^{2}M_{0,r}\right\} \doteq 0,$$

$$(3.9)$$

when computing  $u_{sr}$ ,  $u_{rs}$ ,  $v_{t,sr}$  and  $v_{t,rs}$ . In the case of  $d_v$  velocity dimensions this constraint becomes

$$m_{s}v_{sr}\left[M_{2,s}-u_{sr,i}M_{1i,s}-v_{t,sr}^{2}\left(d_{v}M_{0,s}-\int v_{i}f_{s}\Big|_{v_{i,\min}}^{v_{i,\max}}dS_{i}\right)\right] + m_{r}v_{rs}\left[M_{2,r}-u_{rs}iM_{1i,r}-v_{t,rs}^{2}\left(d_{v}M_{0,r}-\int v_{i}f_{r}\Big|_{v_{i,\min}}^{v_{i,\max}}dS_{i}\right)\right] \doteq 0.$$
(3.10)

We make a final comment that the substitution  $\psi_{\ell} = m_s v^2/2$  is only valid if  $v^2$  belongs to the space spanned by the basis, which for piecewise-linear basis functions (p = 1) it does not. In order for the algorithm to be conservative with p = 1 additional precautions must be taken, a topic that is deferred to Appendix C.

#### 3.3. Discrete relaxation rates

Together with the relations  $u_{sr,i} = u_{rs,i}$  and  $m_s v_{t,sr}^2 = m_r v_{t,rs}^2$ , and the definitions of the collision frequency given in §§ 2.2.1–2.2.2, (3.6) and (3.10) are all one needs to compute the cross-primitive moments for the LBO-EM and LBO-ET. The LBO-G, however, needs to further incorporate the equivalence between the momentum and thermal relaxation rates

of the FPO (2.4) and those of the LBO (2.6) in the discrete sense. First, we obtain the weak form of (2.13) by projecting it onto the  $\psi_{\ell}$  basis function

$$m_{s}v_{sr}\left(M_{1i,s} - u_{sr,i}M_{0,s} + v_{t,sr}^{2} \int f_{s} \Big|_{v_{i,\text{min}}}^{v_{i,\text{max}}} dS_{i}\right) - m_{r}v_{rs}\left(M_{1i,r} - u_{rs,i}M_{0,r} + v_{t,rs}^{2} \int f_{r} \Big|_{v_{i,\text{min}}}^{v_{i,\text{max}}} dS_{i}\right) \doteq \alpha_{E}\left(m_{s} + m_{r}\right)\left(u_{s,i} - u_{r,i}\right), \quad (3.11)$$

where we used the same series of steps that led to (3.6).

The equivalent condition on the thermal relaxation rates necessitates the discrete thermal speed moment of the LBO. We can obtain it by substituting  $\psi_{\ell} = m_s (v - u_s)^2/2$  into the weak scheme in (3.1) and summing over velocity-space cells, resulting in

$$\sum_{k} \int_{K_{j,k}} \frac{m_{s}}{2} (v - u_{s})^{2} \left( \frac{\mathrm{d}f_{s}}{\mathrm{d}t} \right)_{c} dx dv$$

$$= \sum_{k} \int_{x_{j-1/2}}^{x_{j+1/2}} m_{s} v_{sr} \left\{ \left[ \frac{1}{2} (v - u_{s})^{2} G_{s} - (v - u_{s}) v_{t,sr}^{2} \hat{f}_{s} \right] \right|_{v_{k-1/2}}^{v_{k+1/2}}$$

$$- \int_{v_{k-1/2}}^{v_{k+1/2}} \left[ (v - u_{s}) (v - u_{sr}) - v_{t,sr}^{2} \right] f_{s} dv dv. \tag{3.12}$$

Performing the velocity-space integrals, carrying out the k-sum, accounting for the continuity of  $G_s$  and  $\hat{f}_s$  and using the zero-flux boundary conditions on  $G_s$  ushers us to

$$\sum_{k} \int_{K_{j,k}} \left( \frac{\mathrm{d} \left( m_{s} n_{s} v_{t,s}^{2} / 2 \right)}{\mathrm{d}t} \right)_{c} \mathrm{d}x \, \mathrm{d}v$$

$$= \int_{x_{j-1/2}}^{x_{j+1/2}} m_{s} v_{sr} \left\{ \left[ -\left( v - u_{s} \right) v_{t,sr}^{2} f_{s} \right] \Big|_{v_{\min}}^{v_{\max}} - \left[ M_{2,s} - u_{s} M_{1,s} + u_{sr} \left( u_{s} M_{0,s} - M_{1,s} \right) - v_{t,sr}^{2} M_{0,s} \right] \right\} \mathrm{d}x, \tag{3.13}$$

or in the  $d_v$ -dimensional velocity space

$$\sum_{k} \int_{K_{j,k}} \left( \frac{\mathrm{d} \left( m_{s} n_{s} v_{t,s}^{2} / 2 \right)}{\mathrm{d}t} \right)_{c} dx dv$$

$$= \int_{x_{j-1/2}}^{x_{j+1/2}} m_{s} v_{sr} \left\{ v_{t,sr}^{2} \int \left[ -\left( v_{i} - u_{s,i} \right) f_{s} \right] \Big|_{v_{i,\min}}^{v_{i,\max}} dS_{i} \right.$$

$$- \left[ M_{2,s} - u_{s,i} M_{1i,s} + u_{sr,i} \left( u_{s,i} M_{0,s} - M_{1i,s} \right) - v_{t,sr}^{2} d_{v} M_{0,s} \right] \right\} dx, \tag{3.14}$$

where once again the repeated index i implies summation. Equipped with this formula we can write down the discrete equivalence between thermal relaxation rates (2.15) as

$$m_{s}v_{sr} \left\{ v_{t,sr}^{2} \int \left[ -\left(v_{i} - u_{s,i}\right) f_{s} \right] \Big|_{v_{i,\text{min}}}^{v_{i,\text{max}}} dS_{i} \right.$$

$$\left. -\left[ M_{2,s} - u_{s,i} M_{1i,s} + u_{sr,i} \left( u_{s,i} M_{0,s} - M_{1i,s} \right) - v_{t,sr}^{2} d_{v} M_{0,s} \right] \right\}$$

$$\left. - m_{r}v_{rs} \left\{ v_{t,rs}^{2} \int \left[ -\left(v_{i} - u_{r,i}\right) f_{r} \right] \Big|_{v_{i,\text{min}}}^{v_{i,\text{max}}} dS_{i} \right.$$

$$\left. -\left[ M_{2,r} - u_{r,i} M_{1i,r} + u_{rs,i} \left( u_{r,i} M_{0,r} - M_{1i,r} \right) - v_{t,rs}^{2} d_{v} M_{0,r} \right] \right\}$$

$$\left. \dot{=} \alpha_{E} \left[ d_{v} \left( m_{r} v_{t,r}^{2} - m_{s} v_{t,s}^{2} \right) + \frac{m_{r} - m_{s}}{2} \left( u_{s} - u_{r} \right)^{2} \right]. \tag{3.15}$$

The two discrete relaxation rate equivalences in (3.11) and 3.15 in conjunction with the discrete momentum and energy conservation constraints (3.6) and (3.10) provide the four equations for the calculation of the  $u_{sr,i}$ ,  $u_{rs,i}$ ,  $v_{t,sr}$ ,  $v_{t,rs}$  unknowns in the LBO-G, provided a value of  $\beta$ . Equations (3.11) and (3.15), however, are written in terms of the self-primitive moments (e.g.  $u_{s,i}$ ,  $v_{t,s}$ ) of each species, imbuing such equations with some ambiguity as to whether the calculation of self-primitive moments should include the corrections from velocity-space boundaries or not (Hakim *et al.* 2020; Francisquez *et al.* 2020). We therefore opt to instead write those relations in terms of the velocity moments as follows:

$$m_{s}v_{sr}\left(M_{1i,s}-u_{sr,i}M_{0,s}+v_{t,sr}^{2}\int f_{s}\Big|_{v_{t,\min}}^{v_{t,\max}}dS_{i}\right)$$

$$-m_{r}v_{rs}\left(M_{1i,r}-u_{rs,i}M_{0,r}+v_{t,rs}^{2}\int f_{r}\Big|_{v_{t,\min}}^{v_{t,\max}}dS_{i}\right)$$

$$\stackrel{=}{=}\frac{\alpha_{E}\left(m_{s}+m_{r}\right)}{M_{0,s}M_{0,r}}\left(M_{0,r}M_{1i,s}-M_{0,s}M_{1i,r}\right),$$

$$m_{s}v_{sr}\left\{-v_{t,sr}^{2}\int\left(v_{i}-u_{s,i}\right)f_{s}\Big|_{v_{t,\min}}^{v_{t,\max}}dS_{i}\right.$$

$$-\left[M_{2,s}-u_{s,i}M_{1i,s}+u_{sr,i}\left(u_{s,i}M_{0,s}-M_{1i,s}\right)-v_{t,sr}^{2}d_{v}M_{0,s}\right]\right\}$$

$$-m_{r}v_{rs}\left\{-v_{t,rs}^{2}\int\left(v_{i}-u_{r,i}\right)f_{r}\Big|_{v_{t,\min}}^{v_{t,\max}}dS_{i}\right.$$

$$-\left[M_{2,r}-u_{r,i}M_{1i,r}+u_{rs,i}\left(u_{r,i}M_{0,r}-M_{1i,r}\right)-v_{t,rs}^{2}d_{v}M_{0,r}\right]\right\}$$

$$\stackrel{=}{=}\frac{\alpha_{E}}{M_{0,s}M_{0,r}}\left[m_{r}M_{0,s}\left(M_{2,r}-u_{r,i}M_{1i,r}\right)-m_{s}M_{0,r}\left(M_{2,s}-u_{s,i}M_{1i,s}\right)+\frac{m_{r}-m_{s}}{2}\left(u_{s,i}-u_{r,i}\right)\left(M_{0,r}M_{1i,s}-M_{0,s}M_{1i,r}\right)\right].$$

The division by  $M_{0,s}M_{0,r}$  on the right side of these equations is to be performed weakly (Hakim *et al.* 2020) in order to avoid aliasing errors.

# 3.4. Summary of discrete equations

In summary, in order for the algorithm based on (3.1) to conserve momentum and energy the discrete cross-primitive moments are computed using the conservation constraints

$$\begin{split} m_{s}v_{sr}\left(u_{sr,i}M_{0,s}-v_{t,sr}^{2}\int f_{s}\Big|_{v_{i,\text{min}}}^{v_{i,\text{max}}} \mathrm{d}S_{i}\right) \\ &+m_{r}v_{rs}\left(u_{rs,i}M_{0,r}-v_{t,rs}^{2}\int f_{r}\Big|_{v_{i,\text{min}}}^{v_{i,\text{max}}} \mathrm{d}S_{i}\right) \doteq m_{s}v_{sr}M_{1i,s}+m_{r}v_{rs}M_{1i,r}, \\ m_{s}v_{sr}\left[u_{sr,i}M_{1i,s}+v_{t,sr}^{2}\left(d_{v}M_{0,s}-\int v_{i}f_{s}\Big|_{v_{i,\text{min}}}^{v_{i,\text{max}}} \mathrm{d}S_{i}\right)\right] \\ &+m_{r}v_{rs}\left[u_{rs}iM_{1i,r}+v_{t,rs}^{2}\left(d_{v}M_{0,r}-\int v_{i}f_{s}\Big|_{v_{i,\text{min}}}^{v_{i,\text{max}}} \mathrm{d}S_{i}\right)\right] \doteq m_{s}v_{sr}M_{2,s}+m_{r}v_{rs}M_{2,r}. \end{split}$$

$$(3.17)$$

Additionally, the LBO-EM and LBO-ET use  $u_{sr,i} = u_{rs,i}$  and  $m_s v_{t,sr}^2 = m_r v_{t,rs}^2$ , respectively, as well as their corresponding collision frequencies (2.19) and (2.25). When the discrete expansions are inserted in (3.17) one is faced with a linear problem of size  $(d_v + 1)N_b^x$  that must be solved in every position-space cell  $(N_b^x)$  is the number of monomials of the basis spanning position space). The LBO-G on the other hand uses the equality between discrete LBO relaxation rates and the FPO relaxation rates

$$m_{s} v_{sr} \left( u_{sr,i} M_{0,s} - v_{t,sr}^{2} \int f_{s} \Big|_{v_{i,\text{min}}}^{v_{i,\text{max}}} dS_{i} \right) - m_{r} v_{rs} \left( u_{rs,i} M_{0,r} - v_{t,rs}^{2} \int f_{r} \Big|_{v_{i,\text{min}}}^{v_{i,\text{max}}} dS_{i} \right)$$

$$\stackrel{\cdot}{=} m_{s} v_{sr} M_{1i,s} - m_{r} v_{rs} M_{1i,r} + \frac{\alpha_{E} (m_{s} + m_{r})}{M_{0,s} M_{0,r}} \left( M_{0,s} M_{1i,r} - M_{0,r} M_{1i,s} \right), \tag{3.18}$$

$$m_{s}v_{sr}\left\{u_{sr,i}\left(M_{1i,s}-u_{s,i}M_{0,s}\right)+v_{t,sr}^{2}\left[d_{v}M_{0,s}-\int\left(v_{i}-u_{s,i}\right)f_{s}\Big|_{v_{i,\text{min}}}^{v_{i,\text{max}}}dS_{i}\right]\right\}$$

$$-m_{r}v_{rs}\left\{u_{rs,i}\left(M_{1i,r}-u_{r,i}M_{0,r}\right)+v_{t,rs}^{2}\left[d_{v}M_{0,r}-\int\left(v_{i}-u_{r,i}\right)f_{r}\Big|_{v_{i,\text{min}}}^{v_{i,\text{max}}}dS_{i}\right]\right\}$$

$$\stackrel{.}{=}m_{s}v_{sr}\left(M_{2,s}-u_{s,i}M_{1i,s}\right)-m_{r}v_{rs}\left(M_{2,r}-u_{r,i}M_{1i,r}\right)$$

$$+\frac{\alpha_{E}}{M_{0,s}M_{0,r}}\left[m_{r}M_{0,s}\left(M_{2,r}-u_{r,i}M_{1i,r}\right)-m_{s}M_{0,r}\left(M_{2,s}-u_{s,i}M_{1i,s}\right)\right]$$

$$+\frac{m_{r}-m_{s}}{2}\left(u_{s,i}-u_{r,i}\right)\left(M_{0,r}M_{1i,s}-M_{0,s}M_{1i,r}\right)\right],$$
(3.19)

where the relationship between  $\alpha_E$  and  $\nu_{sr}$  is given by (2.7). Therefore for the LBO-G (3.17)–(3.19) signify a  $2(d_v + 1)N_b^x$  linear problem that must be solved in every position-space cell.

## 3.4.1. Discrete equations for the gyroaveraged operator

In § 2.4 we introduced the gyroaveraged cross-species LBO. Its discretization follows that outlined in Francisquez *et al.* (2020) and the calculation of the cross-primitive moments  $u_{\parallel sr}$  and  $v_{t,sr}$  is similar to that done for the non-gyroaveraged operator. The main

differences arise from the fact that moments are defined via  $v_{\parallel}$ - $\mu$  integrals (e.g. (2.37)) and that the momentum density  $M_{1\parallel,s}$  is a scalar instead of a vectorial quantity. The equations that arise from momentum and energy conservation in the gyroaveraged case are thus

$$\begin{split} m_{s} \nu_{sr} \left( M_{1\parallel,s} - u_{\parallel s} r M_{0,s} + v_{t,sr}^{2} \frac{2\pi}{m_{s}} \int \mathcal{J} \hat{f}_{s} \Big|_{\nu_{\parallel \min}}^{\nu_{\parallel \max}} d\mu \right) \\ + m_{r} \nu_{rs} \left( M_{1\parallel,r} - u_{\parallel rs} M_{0,r} + v_{t,rs}^{2} \frac{2\pi}{m_{r}} \int \mathcal{J} \hat{f}_{r} \Big|_{\nu_{\parallel \min}}^{\nu_{\parallel \max}} d\mu \right) \doteq 0, \end{split}$$
(3.20)

$$\begin{split} m_{s} v_{sr} \left[ -v_{t,sr}^{2} \left( 3M_{0,s} - \frac{2\pi}{m_{s}} \int v_{\parallel} \mathcal{J} \hat{f}_{s} \Big|_{v_{\parallel \min}}^{v_{\parallel \max}} d\mu - \frac{2\pi}{m_{s}} \int 2\mu \mathcal{J} \hat{f}_{s} \Big|_{\mu_{\min}}^{\mu_{\max}} dv_{\parallel} \right) \right] \\ + m_{r} v_{rs} \left[ M_{2,r} - u_{\parallel rs} M_{1\parallel,r} \right. \\ \left. - v_{t,rs}^{2} \left( 3M_{0,r} - \frac{2\pi}{m_{r}} \int v_{\parallel} \mathcal{J} \hat{f}_{r} \Big|_{v_{\parallel \min}}^{v_{\parallel \max}} d\mu - \frac{2\pi}{m_{r}} \int 2\mu \mathcal{J} \hat{f}_{r} \Big|_{\mu_{\min}}^{\mu_{\max}} dv_{\parallel} \right) \right] \doteq 0. \end{split}$$
(3.21)

For the gyroaveraged LBO-EM and LBO-ET (3.20)–(3.21), and the relations  $u_{\parallel sr} = u_{\parallel rs}$  and  $m_s v_{t,sr}^2 = m_r v_{t,rs}^2$ , is all that is needed to compute the cross-primitive moments. This requires a solution to a linear problem of size  $2N_b^x$  in each position-space cell. In the case of the LBO-G operator we make use of the discrete moment relaxation equations once again, as in (3.18)–(3.19) but using the gyroaveraged moments instead

$$m_{s} \nu_{sr} \left( u_{\parallel s} r M_{0,s} - \nu_{t,sr}^{2} \frac{2\pi}{m_{s}} \int \mathcal{J} \hat{f}_{s} \Big|_{\nu_{\parallel \min}}^{\nu_{\parallel \max}} d\mu \right)$$

$$- m_{r} \nu_{rs} \left( u_{\parallel rs} M_{0,r} - \nu_{t,rs}^{2} \frac{2\pi}{m_{r}} \int \mathcal{J} \hat{f}_{r} \Big|_{\nu_{\parallel \min}}^{\nu_{\parallel \max}} d\mu \right)$$

$$\dot{=} m_{s} \nu_{sr} M_{1\parallel,s} - m_{r} \nu_{rs} M_{1\parallel,r} + \frac{\alpha_{E} (m_{s} + m_{r})}{M_{0,s} M_{0,r}} \left( M_{0,s} M_{1\parallel,r} - M_{0,r} M_{1\parallel,s} \right), \qquad (3.22)$$

$$\begin{split} m_{s}\nu_{sr} \left\{ u_{\parallel sr} \left( M_{1\parallel,s} - u_{\parallel s} M_{0,s} \right) \\ + v_{t,sr}^{2} \left[ 3M_{0,s} - \frac{2\pi}{m_{s}} \int \left( v_{\parallel} - u_{\parallel s} \right) \mathcal{J} \hat{f}_{s} \Big|_{v_{\parallel \min}}^{v_{\parallel \max}} d\mu - \frac{2\pi}{m_{s}} \int 2\mu \mathcal{J} \hat{f}_{s} \Big|_{\mu_{\min}}^{\mu_{\max}} d\nu_{\parallel} \right] \right\} \\ - m_{r}\nu_{rs} \left\{ u_{\parallel rs} \left( M_{1\parallel,r} - u_{\parallel r} M_{0,r} \right) \right. \\ \left. + v_{t,rs}^{2} \left[ 3M_{0,r} - \frac{2\pi}{m_{r}} \int \left( v_{\parallel} - u_{\parallel r} \right) \mathcal{J} \hat{f}_{r} \Big|_{v_{\parallel \min}}^{v_{\parallel \max}} d\mu - \frac{2\pi}{m_{r}} \int 2\mu \mathcal{J} \hat{f}_{r} \Big|_{\mu_{\min}}^{\mu_{\max}} d\nu_{\parallel} \right] \right\} \\ \dot{=} m_{s}\nu_{sr} \left( M_{2,s} - u_{\parallel s} M_{1\parallel,s} \right) - m_{r}\nu_{rs} \left( M_{2,r} - u_{\parallel r} M_{1\parallel,r} \right) \end{split}$$

$$+\frac{\alpha_{E}}{M_{0,s}M_{0,r}}\left[m_{r}M_{0,s}\left(M_{2,r}-u_{\parallel r}M_{1\parallel,r}\right)-m_{s}M_{0,r}\left(M_{2,s}-u_{\parallel s}M_{1\parallel,s}\right)\right.\\ +\frac{m_{r}-m_{s}}{2}\left(u_{\parallel s}-u_{\parallel r}\right)\left(M_{0,r}M_{1\parallel,s}-M_{0,s}M_{1\parallel,r}\right)\right],$$
(3.23)

where once again weak division by  $M_{0,s}M_{0,r}$  on the right-hand side of these equations assumed (Hakim *et al.* 2020) in order to avoid aliasing errors. In (3.20)–(3.23) we assumed a  $v_{\parallel}$ - $\mu$  simulation such that  $d_v=3$ . For a  $v_{\parallel}$  simulation the 3 in front of  $M_{0,s}$  and  $M_{0,r}$  would be simply a 1,  $(2\pi/m)\int d\mu$  integrals would vanish and so would the the  $2\mu\mathcal{J}\hat{f}$  terms. In either case, the gyroaveraged LBO-G requires inverting a matrix with  $4N_b^x \times 4N_b^x$  matrix in each configuration space cell.

#### 4. Benchmarks and results

The algorithm introduced in § 3 has been implemented in the DG Vlasov–Maxwell (Juno *et al.* 2018; Hakim & Juno 2020) and gyrokinetic (Shi *et al.* 2019; Mandell *et al.* 2020) solvers of the Gkeyll computational plasma physics framework (Gkeyll 2020). In order to demonstrate the algorithm's properties and test the implementation we have run a number of tests and we here present the results of three of them: § 4.1 contains basic tests showing the conservative properties of the algorithm, § 4.2 contains four dimensional Vlasov–Maxwell simulations of collisional Landau damping of an electron plasma wave and § 4.3 uses the gyrokinetic solver to explore velocity and temperature relaxation. All the input files used to generate these results are available online (see Appendix A).

## 4.1. Conservation tests

# 4.1.1. Vlasov LBO conservation

We check that momentum and energy are indeed conserved by our discrete scheme by initiating two populations of electrons and protons with an arbitrary non-Maxwellian distribution function given by

$$f_s(\mathbf{v}, t = 0) = a [1 + d\cos(k_s v)] \exp\left[-\frac{(\mathbf{v} - \mathbf{b}_s)^2}{2\sigma_s^2}\right],$$
 (4.1)

with  $a=7\times 10^{19}$ , d=0.5,  $k_s=\pi/v_{t,s}$ ,  $\sigma_s=v_{t,s}$ ,  $b_e=\{v_{t,e}/2,-v_{t,e}/2,0\}$ ,  $b_i=\{3v_{t,i}/2,3v_{t,i}/2,v_{t,i}/2\}$  with  $v_{t,s}=\sqrt{T_{s0}/m_s}$ , and  $T_{e0}=40$  eV and  $T_{i0}=80$  eV. We discretize these distribution functions in phase spaces restricted to  $[-1,1]\times [-5v_{t,s},5v_{t,s}]^{d_v}$  and meshed with  $1\times N_v^{d_v}$  cells. We show conservation properties for both piecewise-linear (p=1) and piecewise-quadratic (p=2) serendipity basis functions (Juno *et al.* 2018); higher-order basis functions may also be used but the results do not change. For the same reason we use a single cell in position space; the results in this section are independent of position-space dimensionality although we checked such cases anyway to make sure there are no errors in the implementation.

We time integrate the cross-species collision terms (no self-species collisional or collisionless terms are included here) with constant collision frequency using a strong-stability preserving (SSP) third-order Runge–Kutta method (RK3). As electrons and ions collide with each other their temperatures and flow velocities relax to a common value, a process that is more carefully benchmarked in § 4.3. We also see that whatever anisotropies were present at t=0 go away on the  $\nu_{sr}^{-1}$  time scale. In figure 1, for example, we illustrate the isotropization of the electrons after several  $(\nu_{ei}^{M})^{-1}$  periods as they collide with the ions using the LBO-EM, but since  $\nu_{ie}$  is smaller by  $m_e/m_i$  the ions will take much longer to isotropize as they collide with the electrons.

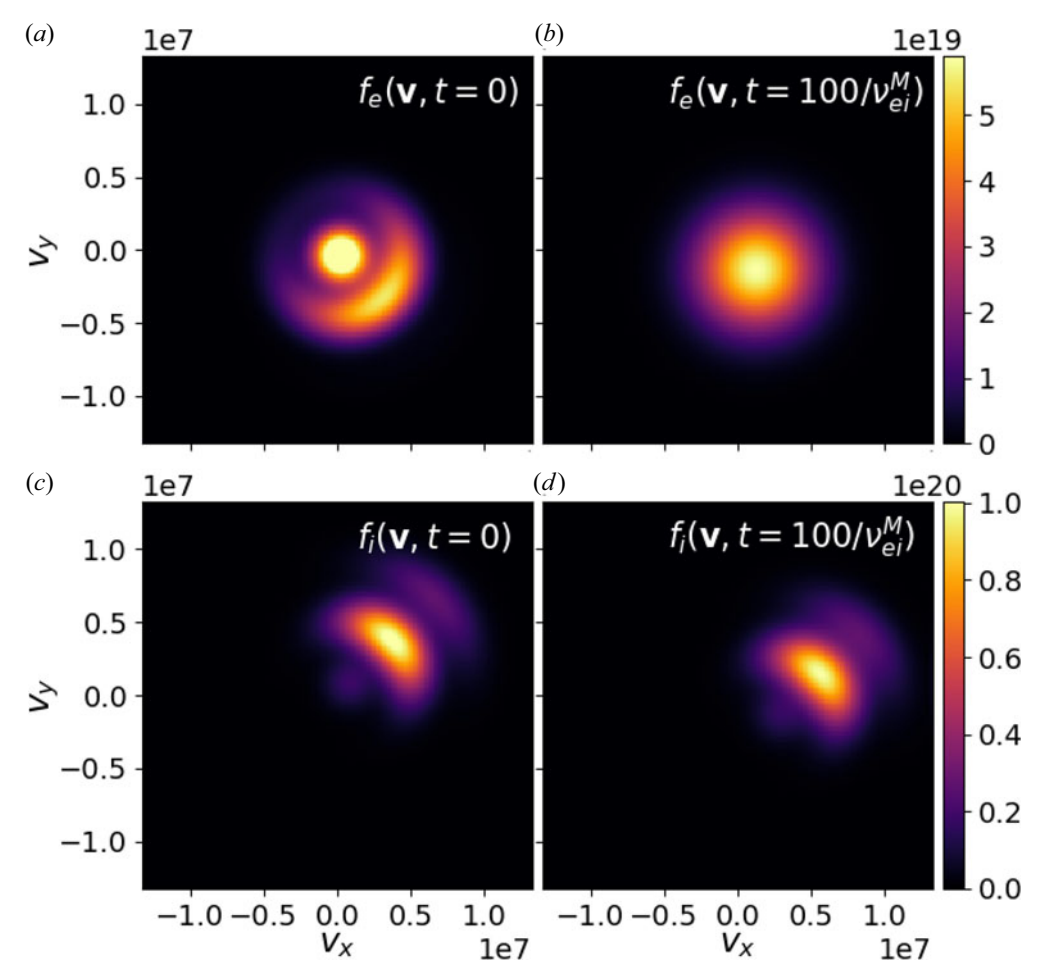


FIGURE 1. Initial and final (after  $v_{ei}^M t = 100$ ) electron and ion distribution functions as they collide with each other with the LBO-EM model using  $1 \times 64^2$  cells and a p = 2 serendipity basis. Initial conditions are given in (4.1). Colour bars are normalized to the extrema at  $v_{ei}^M t = 100$ .

We ran this simulation for  $d_v = \{1, 2, 3\}$ ,  $p = \{1, 2\}$  and using both the LBO-EM and the LBO-G. The ability to conserve the first three volume-integrated velocity moments of the distribution function was quantified in each case by integrating the equations for  $N_t$  time steps, and computing the relative error per time step in the volume-integrated particle, momentum and kinetic energy density. The relative error per time step in the number density  $M_0$  is given by

$$E_{r,M_0} = \frac{1}{N_t} \frac{\langle M_{0e} + M_{0i} \rangle (t = N_t \Delta t) - \langle M_{0e} + M_{0i} \rangle (t = 0)}{\langle M_{0e} + M_{0i} \rangle (t = 0)},$$
(4.2)

where  $\langle \cdot \rangle$  indicates a volume average and  $N_t = 10^4$ . The relative error per time step in momentum and kinetic energy conservation takes into account the mass of each species

$$E_{r,M_{1k}} = \frac{1}{N_t} \frac{\langle m_e M_{1e,k} + m_i M_{1i,k} \rangle (t = N_t \Delta t) - \langle m_e M_{1e,k} + m_i M_{1i,k} \rangle (t = 0)}{\langle m_e M_{1e,k} + m_i M_{1i,k} \rangle (t = 0)}, \tag{4.3}$$

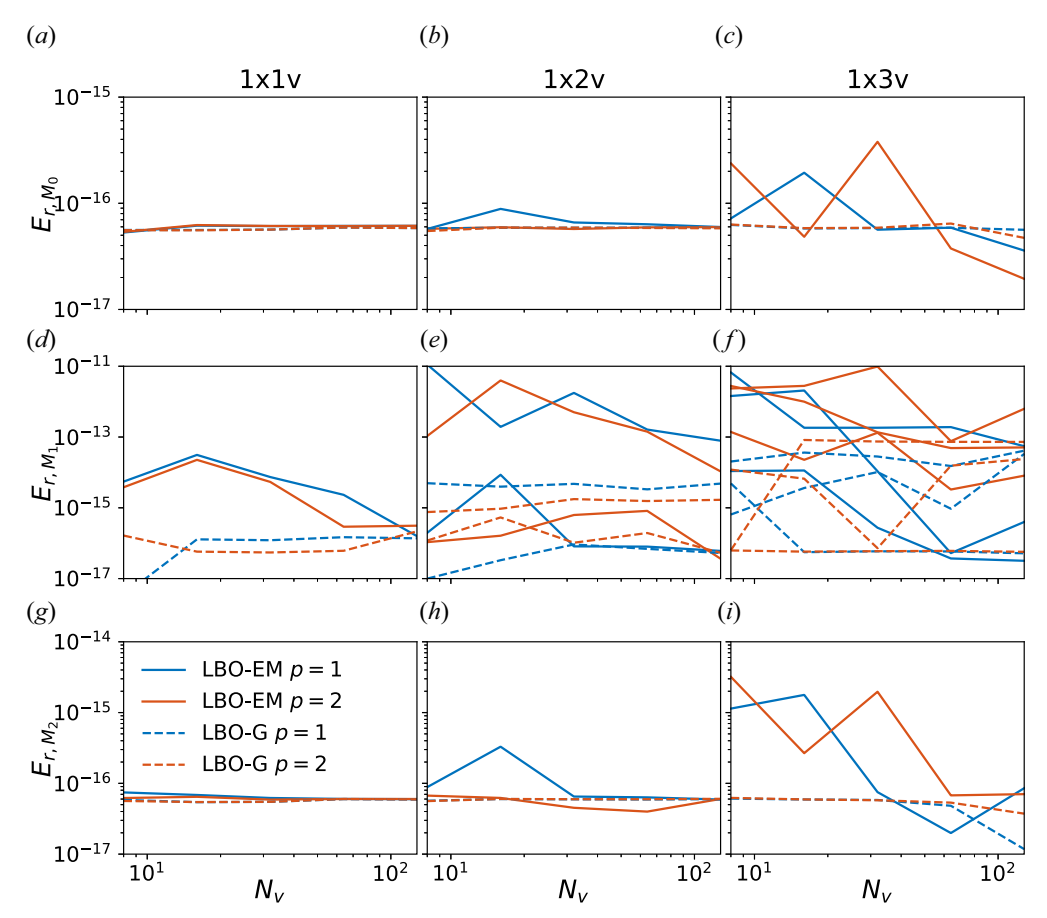


FIGURE 2. Relative error per time step in number density (a-c), momentum density in each direction (d-f) and kinetic energy density (g-i). The middle row plots contain  $d_v$  lines for each operator and p, corresponding to the error per time step in the conservation of momentum along each direction.

$$E_{r,M_2} = \frac{1}{N_t} \frac{\left\langle \frac{1}{2} m_e M_{2e} + \frac{1}{2} m_i M_{2i} \right\rangle (t = N_t \Delta t) - \left\langle \frac{1}{2} m_e M_{2e} + \frac{1}{2} m_i M_{2i} \right\rangle (t = 0)}{\left\langle \frac{1}{2} m_e M_{2e} + \frac{1}{2} m_i M_{2i} \right\rangle (t = 0)}.$$
 (4.4)

The results as a function of velocity-space resolution (i.e.  $N_v$ ) are given in figure 2. The middle row plots have  $d_v$  lines for each operator and polynomial order p because the relative error per time step in the volume-integrated momentum density is measured along each direction separately. In all cases we see that the errors in momentum conservation per time step remain of the order of machine precision. This is true even for the simulations with piecewise-linear basis functions or very coarse velocity-space meshes. The LBO-ET uses the same algorithm and implementation as LBO-EM but with a different collision frequency, so its conservation errors are similar to those of the LBO-EM shown here.

These conservation properties do not depend on the large mass disparity between ions and electrons; the algorithm's ability to conserve the velocity moments is also independent of the mass ratio. We provide as an example the  $d_v = 2$  and p = 2 simulation with the LBO-EM, scanning the number of velocity-space cells in one direction  $(N_v)$  and using the mass ratios  $m_i/m_e = \{300, 600, 1000, 1836\}$ . The conservation errors for

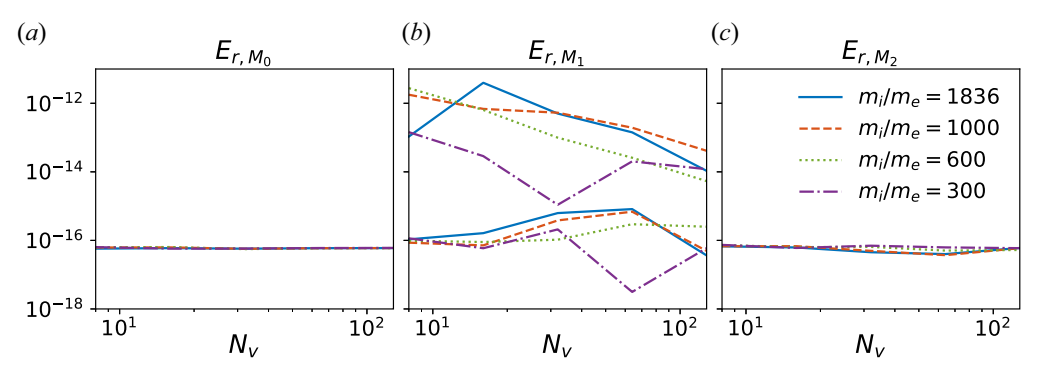


FIGURE 3. Relative error per time step in number density (a), momentum density in each direction (b) and kinetic energy density (c) in two-dimensional velocity space ( $d_v = 2$ ).

these simulations are provided in figure 3, once again shown that for all mass ratios and resolutions used, the error per time step in the volume-integrated velocity moments remains of the order of machine precision.

# 4.1.2. Gyroaveraged LBO conservation

Similar tests were run with the gyroaveraged version of the LBO operators in order to guarantee that the algorithm remains conservative in that case as well. For these tests we initialize the ion and electron distribution functions with

$$f_s(v_{\parallel}, \mu, t = 0) = \frac{a \left[1 + d \cos(k_s v)\right]}{\left(2\pi\sigma_s^2\right)^{3/2}} \exp\left[-\frac{\left(v_{\parallel} - b_s\right)^2 + 2\mu B m_s}{2\sigma_s^2}\right],\tag{4.5}$$

and the parameters B=1.2 T,  $a=7\times 10^{19}$ , d=0.5,  $k_s=\pi/v_{t,s}$ ,  $\sigma_s=v_{t,s}$ ,  $b_e=5v_{t,i}/4$ ,  $b_i=v_{t,i}$ ,  $v_{t,s}=\sqrt{T_{s0}/m_s}$ ,  $T_{e0}=40$  eV and  $T_{i0}=80$  eV. The phase space  $[-1,1]\times [-5v_{t,s},5v_{t,s}]\times [0,m_s(5v_{t,s})^2/(2B)]$  is meshed with  $1\times N_v^2$  cells and functions are expanded on piecewise-linear (p=1) or piecewise-quadratic (p=2) serendipity basis.

We allow the electrons and ions to collide with each other but not with themselves, and we do not apply the collisionless terms either. The cross-species collision terms were integrated in time for  $10^4$  time steps using a third-order SSP RK3, and we computed the relative error per time step in the volume-integrated velocity moments as in § 4.1.2. The results in figure 4 demonstrate how the relative error per time step in the conservation of velocity moments stays of order of machine precision for all velocity-space resolutions, and even for p = 1. Figure 4 gives conservation errors for the LBO-ET and the LBO-G; the LBO-EM has similar conservative properties as the LBO-ET since it only differs by the definition of the collision frequency.

# 4.2. Landau damping of electron Langmuir waves

A seminal test bed for collision operators is the Landau damping of plasma waves across the collisional range. We pursued this analysis to examine the effect that these collision models have on the Landau damping rate of electrostatic electron Langmuir waves. For this purpose we employ the Vlasov–Maxwell solver in Gkeyll (Juno *et al.* 2018; Hakim & Juno 2020) with the self-species collision terms (Hakim *et al.* 2020) and the multispecies collision models described in this work. The hydrogen ions are fixed in time so the

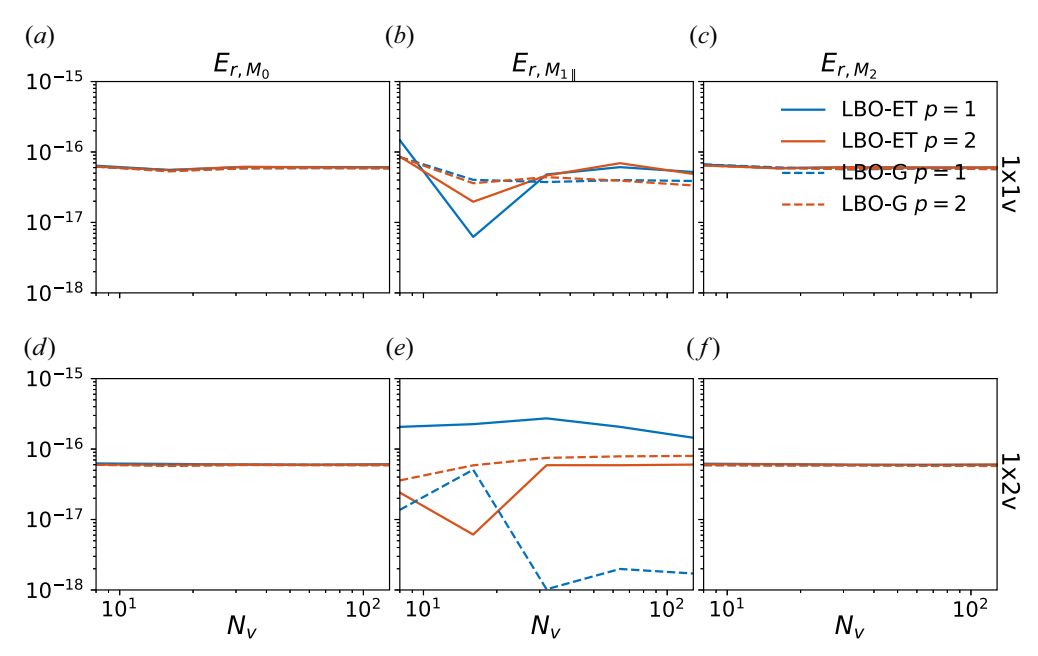


FIGURE 4. Relative error per time step in number density (a,b), momentum density (c,d) and kinetic energy density (e,f) as a function of the number of cells along one direction of velocity space  $(N_v)$  for the gyroaveraged LBO-ET (solid) and LBO-G (dashed). Top row contains tests with  $v_{\parallel}$ -space only, while the bottom row contains tests in  $v_{\parallel} - \mu$  space.

equations solved are

$$\frac{\partial f_e}{\partial t} + \boldsymbol{v} \cdot \nabla f_e - \boldsymbol{E} \cdot \nabla_{\boldsymbol{v}} f_e = \sum_{r=e,i} v_{er} \nabla_{\boldsymbol{v}} \cdot \left[ (\boldsymbol{v} - \boldsymbol{u}_{er}) f_e + v_{ter}^2 \nabla_{\boldsymbol{v}} f_e \right], \tag{4.6}$$

$$\frac{\partial E}{\partial t} = -J,\tag{4.7}$$

where we used normalized units,<sup>4</sup> the current density is given by  $J = -M_{1e}$  and we solve (4.7) in a way that keeps the simulation electrostatic.<sup>5</sup> We use four-dimensional simulations with the phase space  $[-\pi/k, \pi/k] \times [-5v_{t,e}, 5v_{t,e}]^3$  discretized by  $16 \times 36^3$  cells and p = 2 basis functions, for the wavenumber  $k\lambda_{De} = 0.3$ , with  $\lambda_{De}$  being the electron Debye length. We confirmed that the resolution used is the minimum needed to obtain converged results by scanning the position- and velocity-space resolution as well as the velocity-space extents. The static ions have the normalized density  $n_i(x) = 1$  while the electrons are initialized with a non-drifting Maxwellian distribution that has the temperature  $T_e = 1 = T_i$  and the density  $n_e(x, t = 0) = 1 + \alpha \cos(kx)$ , with  $\alpha = 10^{-4}$ . The electric field is initialized in a manner consistent with Poisson's equation  $E = -\hat{x}\alpha\sin(kx)/k$ .

As the simulation proceeds we see the amplitude of the electrostatic wave damp, which can be appreciated by examining the volume-integrated field energy over time as shown in figure 5(a). We can quantify the rate at which these waves damp and plot it as a function of

<sup>&</sup>lt;sup>4</sup>https://gkeyll.readthedocs.io/en/latest/dev/vlasov-normalizations.html.

<sup>&</sup>lt;sup>5</sup>http://ammar-hakim.org/sj/je/je33/je33-buneman.html.

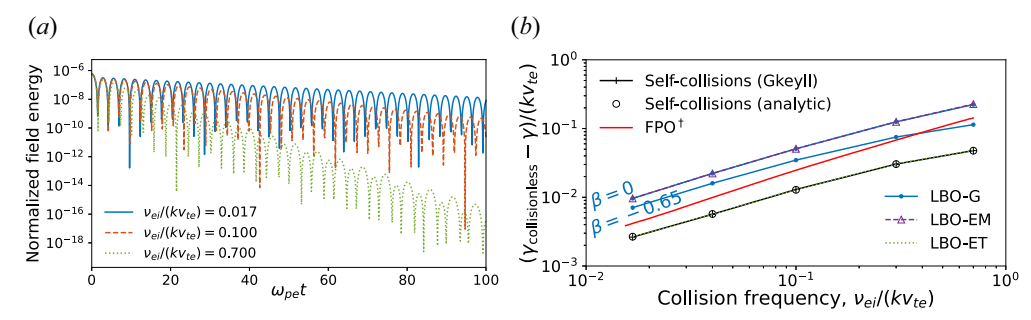


FIGURE 5. (a) Normalized volume-integrated field energy in simulations of electron Langmuir waves as they Landau damp over time. (b) Damping rates of electron Langmuir waves given as the offset from the collisionless value of  $\gamma_{\text{collisionless}}/\omega_{pe} = -1.247 \times 10^{-2}$  for the LBO-G with  $\beta = 0$  and  $\beta = -0.65$  (blue circles), the LBO-EM (purple triangles) and the LBO-ET (dotted green) compared with those with a full FPO (Jorge *et al.* 2019) (solid red). If using only self-collisions, numerical Gkeyll data (black crosses) agrees with theory (black circles).

collision frequency as is done in figure 5(*b*). If one were to only use self-species collisions one would obtain the results shown with black crosses, and for that case the equations are sufficiently simple that one can obtain an analytic dispersion relation (Anderson & O'Neil 2007; Francisquez *et al.* 2020) which agrees well with the numerical results (black circles), providing additional confidence in the Gkeyll implementation. When we introduce electron–ion collisions obtaining analytic growth rates is more difficult. So we instead compare the results obtained with the LBO-G (solid blue), the LBO-EM (dashed purple) and the LBO-ET (dotted green) with previously reported results for the FPO (Jorge *et al.* 2019).

The LBO-G simulations were performed using  $v_{ei}^G = \sqrt{2}v_{ee}$  (=  $(m_i/m_e)v_{ie}$ ) since this is the relationship assumed in the reference FPO work (Jorge *et al.* 2019). Figure 5(b) suggests that the LBO-G can provide a more accurate description of this kinetic phenomenon than, say, using self-species collisions only. There is the caveat, however, that we have not established from first principles what the most suitable choice of the free parameter  $\beta$  ought to be at any given collision frequency. We scanned this parameter and show the results for  $\beta = 0$  and  $\beta = -0.65$ , the latter bringing the damping rates closer to those of the full FPO. But it is apparent that the wrong choice of  $\beta$  can also result in significant deviation from the FPO.

Also shown in figure 5(b) are the damping rates obtained when using the LBO-EM and the LBO-ET. Despite having a different model for  $u_{sr}$  and  $v_{t,sr}$ , LBO-EM has the same collision frequency ( $v_{ei}^M = v_{ei}^G(\beta = 0)$ ) and gives the same damping rates as the LBO-G with  $\beta = 0$  (top blue and dashed purple lines). The LBO-ET on the other hand has a collision frequency that is smaller by the mass ratio ( $v_{ei}^T = m_e v_{ei}^M/(m_e + m_i) \simeq (m_e/m_i)v_{ei}^M$ ), and therefore is essentially equivalent to neglecting cross-species collisions for this problem; i.e. solid black and dotted green lines agree. If we were to run the simulation with the LBO-ET but the same value of  $v_{ei}$  as the LBO-EM then we would simply obtain the same results as if we had used the LBO-EM.

## 4.3. *Velocity and temperature relaxation*

As a final benchmark of the multispecies LBO algorithms and solvers we employ the gyroaveraged LBO to model the relaxation of a deuterium plasma to thermal equilibrium. We employ identical conditions, as best as we can tell, to those used in a benchmark of the

FPO in the XGC code (Hager *et al.* 2016). The same test was recently performed with a finite-volume implementation of the LBO-ET and LBO-EM in GENE-X Ulbl *et al.* (2021). This means that the initial distribution functions are described by the bi-Maxwellians

$$f_s\left(v_{\parallel}, \mu, t = 0\right) = \frac{n_0}{\alpha \left(2\pi v_{t,s}^2\right)^{3/2}} \exp\left[-\frac{\left(v_{\parallel} - u_{\parallel s}\right)^2 + 2\mu B/(m_s \alpha)}{2v_{t,s}^2}\right],\tag{4.8}$$

where B=1 T,  $v_{t,s}=\sqrt{T_{s0}/m_s}$   $\alpha=1.3$ ,  $u_{\parallel i}=50(m_e/m_i)v_{t,i}$ ,  $u_{\parallel e}=0.5\sqrt{m_e/m_i}v_{t,s}$ ,  $T_{i0}=200$  eV and  $T_{e0}=300$  eV. Note that these reference temperatures are slightly different than the true initial temperatures  $T_i(t=0)=240$  eV and  $T_e(t=0)=360$  eV given by  $T_s=(2T_{\perp s}+T_{\parallel s})/3$ . For this test we once again neglect the collisionless terms and use a collision frequency that depends on time, i.e.  $v_{sr}=v_{sr}(T_s(t),T_r(t))$ . The phase space  $[-2,2]\times[-5v_{t,s},5v_{t,s}]\times[0,m_s(5v_{t,s})^2/(2B)]$  is meshed with  $1\times16^2$  cells and dynamic fields are expanded in a piecewise-linear (p=1) basis. This resolution and velocity-space extents were confirmed as sufficient by convergence tests.

Figure 6 provides the time evolution of the parallel and perpendicular temperatures for the LBO-G ( $\beta = 0$ ), LBO-EM and LBO-ET operators compared with the previously reported FPO results<sup>6</sup> (Hager *et al.* 2016). The first event is the isotropization of the electrons followed by the isotropization of the ions, happening on the  $v_{ss}^{-1}$  time scale. We used

$$\nu_{ss} = \frac{1}{\sqrt{2}} \frac{q_s^4 n_s \log \Lambda_{ss}}{3 (2\pi)^{3/2} \epsilon_0^2 m_s^2 v_{ts}^3},\tag{4.9}$$

for the like-species scattering rate. Note that the LBO-G and LBO-EM exhibit a delayed isotropization time compared with the FPO's, an observation that Pezzi, Valentini & Veltri (2015) had also made while comparing the self-species Dougherty operator with the FPO (in Landau form). Later, on the  $v_{ie}^{-1}$  time scale, we see the electrons and ions come into thermal equilibrium with each other, a process that is better described by both the LBO-G and the LBO-ET operators since, after all, the LBO-EM made no attempt at matching the FPO thermal relaxation rates. The time axis on these plots has been normalized to the isotropization rate (Huba 2013)

$$\nu_T^i = \frac{2\sqrt{\pi}q_i^4 n_i \log \Lambda_{ii}}{(4\pi\epsilon_0)^2 m_i^2 \nu_{t,i}^3} A^{-2} \left[ -3 + (A+3) a_F \right], \tag{4.10}$$

where  $v_{t,i}$  and  $\log \Lambda_{ii}$  use the initial ion temperature (240 eV), and  $A = T_{\perp i}/T_{\parallel i} - 1$  and  $a_F = A^{-1/2} \tan^{-1}(A^{1/2})$  if A > 0 or  $a_F = (-A)^{1/2} \tanh^{-1}(-A)^{1/2}$  if A < 0.

We can also examine the velocity evolution as the plasma approaches an equilibrium as is done in figure 7. The first thing we notice is that the LBO-ET (green dash-dot with circles) grossly overestimates the time scale on which the electron flow relaxes to the ion flow, which happens because the ions are so much more massive. By definition the LBO-ET did not attempt to match the momentum relaxation rate, and we see the result of that here. On the other hand, the LBO-G (solid blue) and LBO-EM (dashed orange with crosses) models do a better job of approximating the FPO results for the slowing down of electrons, since their formulation included matching the FPO's momentum relaxation rates. There is still a discrepancy, e.g. between solid blue and dashed orange lines, although

<sup>&</sup>lt;sup>6</sup>Note that the FPO results here (and those in figure 7) have been shifted in time by  $-\Delta t = 3.85783 \times 10^{-7}$  s compared with those in Hager *et al.* (2016), since that work shifted them by  $\Delta t$  in order to show the results with a logarithmic *x*-axis.

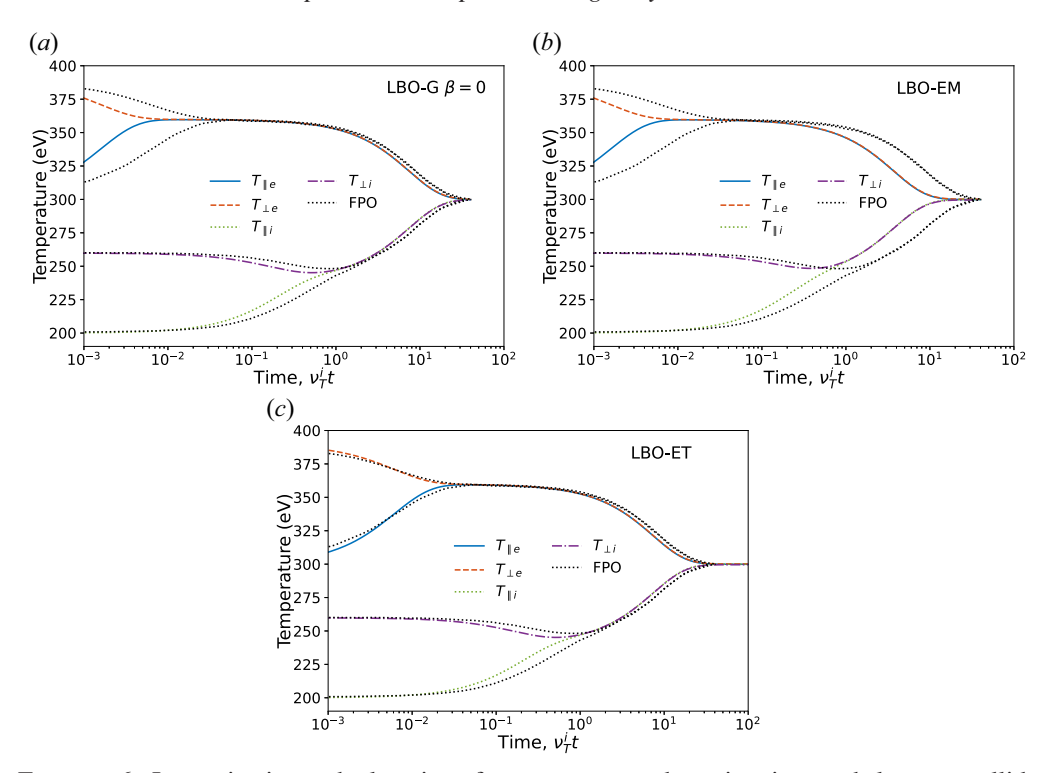


FIGURE 6. Isotropization and relaxation of temperatures as deuterium ions and electrons collide with themselves and each other, compared with the results from the full FPO (Hager *et al.* 2016). (a) LBO-G with  $\beta = 0$ . (b) LBO-EM. (c) LBO-ET.

we point out that the LBO-G and LBO-EM would appear to match the analytic result based on the flow relaxation frequency given by the friction force at large mass ratio (Hinton & Hazeltine 1976) (see figure 4 of Hager *et al.* 2016).

### 5. Conclusion

This work presented three separate formulations of full-f nonlinear multispecies collisions based on the model Lenard–Bernstein or Dougherty operator (LBO), following the ideas Greene (1973) and Haack *et al.* (2017) employed for the BGK operator. This resulted in the LBO-G, LBO-EM and LBO-ET operators, each providing different formulas for the cross-species primitive moments  $u_{sr,i}$  and  $v_{t,sr}$  and collision frequency  $v_{sr}$ . The LBO-G attempts to exactly match the thermal and momentum relaxation rates of the FPO, but it introduces a free parameter  $\beta$ . The LBO-EM only matches the FPO momentum relaxation rate, while the LBO-ET only tries to approximately match the FPO thermal relaxation rate. Gyroaveraged versions of this operator were also provided in this work, which may be used in long-wavelength gyrokinetic models. Compared with previous works, the multispecies LBO model presented here has the following advantages:

- (i) It is suitable for arbitrary mass ratios.
- (ii) Some pathologies, such as negative cross-species temperatures (possible in the BGK operator of Greene 1973), are avoided.
- (iii) It conserves energy and momentum exactly.
- (iv) It approximately reproduces the FPO's momentum and thermal relaxation rates.

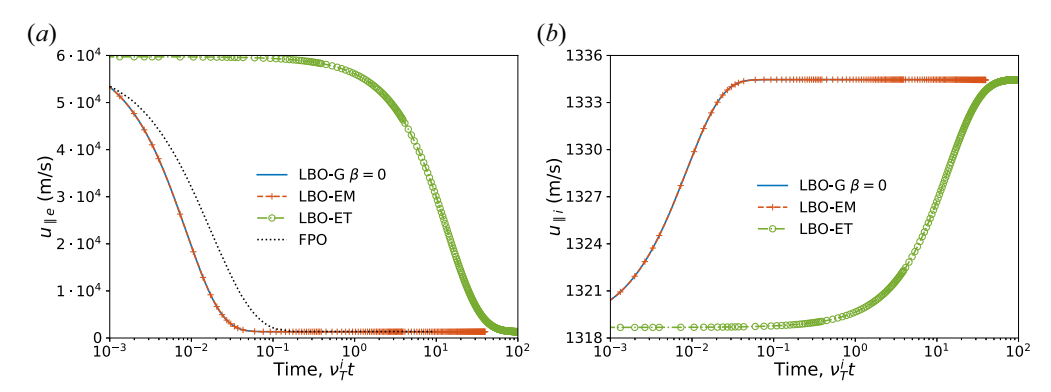


FIGURE 7. Relaxation of parallel flow speed as deuterium ions and electrons collide with themselves and each other. Electron flow speeds are compared with the results from the full FPO (dotted black, Hager *et al.* (2016)). Flow speeds when using the LBO-G ( $\beta=0$ ) are given in solid dark blue, results for the LBO-EM in dashed orange with crosses and green dash-dot lines with circles represent results obtained with the LBO-ET.

# (v) A proof of non-decreasing entropy (the *H* theorem) exists.

These multispecies LBO models may also be discretized for numerical implementation using a DG method in the spirit of Hakim *et al.* (2020) and Francisquez *et al.* (2020). We provided an algorithm for a DG discretization of such operators based on weak projections and the recovery of discontinuous derivatives across cell boundaries (Hakim *et al.* 2020). The primary focus of this work was, however, the computation of the cross-primitive moments  $u_{sr,i}$  and  $v_{t,sr}$  in a manner that results in an exactly conservative algorithm, i.e. capable of conserving particle, momentum and kinetic energy density independently of resolution. This property was accomplished by solving a weak system of equations consisting of the discrete equivalent of momentum and energy conservation, and in the case of the LBO-G, a discrete equivalent of the momentum and thermal relaxation rate constraints. Discrete conservation was also attained when piecewise-linear basis functions (p=1) were used by carefully employing the projection of  $v^2$  onto the basis (or  $v_{\parallel}^2$  for the gyroaveraged operator).

Our tests indicate that the implementation in Gkeyll exhibits this exact conservation feature, for all the velocity dimensions and polynomial orders tested. Exact conservation was also confirmed in Gkeyll's gyroaveraged solver for one and two velocity dimensions. In addition we combined the LBO solver with Gkeyll's Vlasov–Maxwell solver and examined the impact that LBO cross-species collisions has on the Landau damping rates of electron Langmuir waves. Due to the definition of the LBO-ET collision frequency, such operator gave no improvements over using self-species collisions only, while the LBO-G and LBO-EM gave slightly more accurate descriptions of this phenomenon. The LBO-G can be made to agree more with the FPO by choosing a different value of  $\beta$ , but we have not presented a first-principles model for that free parameter yet. Despite this unspecified parameter, the LBO-G operator has been in use by Gkeyll's Vlasov and gyrokinetic solvers for quite some time now. For example, recent Vlasov–Maxwell simulations using this operator showed the inhibition of magnetic dynamo due to Landau damping (Pusztai *et al.* 2020). Nevertheless, this  $\beta$  parameter will be the focus of follow up work.

Lastly, we benchmarked the gyroaveraged multispecies LBO by simulating a system in which ions and electrons are anisotropic, drifting relative to each other and out of thermal equilibrium. The LBO-EM and LBO-ET each do better at approximating the

FPO's velocity and temperature evolution, as their formulation would predict. The LBO-G is perhaps the best choice here, since it does well at matching the temperature evolution and provides the same level of accuracy when it comes to the velocity relaxation as the LBO-EM.

# Acknowledgements

We express our gratitude towards R. Jorge and R. Hager for clarifying how the FPO results were obtained, as well as our gratitude for the other members of the Gkeyll team who aided this work. We used the Stellar cluster at Princeton University and the Cori cluster at the National Energy Research Scientific Computing Center (NERSC), a U.S. Department of Energy Office of Science User Facility. M.F., A.H. and G.W.H. were supported by the Partnership for Multiscale Gyrokinetic Turbulence (MGK) and the High-Fidelity Boundary Plasma Simulation (HBPS) projects, part of the U.S. Department of Energy (DOE) Scientific Discovery Through Advanced Computing (SciDAC) program, and the DOE's ARPA-E BETHE program, via DOE contract DE-AC02-09CH11466 for the Princeton Plasma Physics Laboratory. J.J was supported by a NSF Atmospheric and Geospace Science Postdoctoral Fellowship (Grant No. AGS-2019828). M.F., as well as D.R.E., were also supported by the Partnership for Multiscale Gyrokinetic Turbulence (MGK) (subaward No. UTA18-000276 to M.I.T. under U.S. DOE Contract DE-SC0018429).

Editor William Dorland thanks the referees for their advice in evaluating this article.

#### Declaration of interests

The authors report no conflict of interest.

# Data availability statement

The data that support the findings of this study are openly available in Zenodo at https://doi.org/10.5281/zenodo.6350748.

## Appendix A. Getting Gkeyll and reproducing results

Readers may reproduce our results and also use Gkeyll for their applications. The code and input files used here are available online. Full installation instructions for Gkeyll are provided on the Gkeyll website Gkeyll (2020). The code can be installed on Unix-like operating systems (including Mac OS and Windows using the Windows Subsystem for Linux) either by installing the pre-built binaries using the conda package manager (https://www.anaconda.com) or building the code via sources. The input files used here are under version control and can be found at https://github.com/ammarhakim/gkyl-paper-inp/tree/master/2021\_JPP\_crossLBO.

## Appendix B. *H*-theorem proof

In this section we show that the improved interspecies Dougherty collisions do not decrease total entropy given the cross-species primitive moments for collisions between

species s and species r(2.8)–(2.9). The rate of change of the entropy S can be written as

$$\frac{\partial S}{\partial t} = -\frac{\partial}{\partial t} \sum_{s} \int d^{d_{v}} v f_{s} \ln f_{s}$$

$$= -\sum_{s} \int d^{d_{v}} v \frac{\partial f_{s}}{\partial t} (\ln f_{s} + 1) ,$$

$$= -\sum_{s} \int d^{d_{v}} v v_{sr} (\div v J_{sr}) (\ln f_{s} + 1) ,$$
(B1)

where  $J_{sr} = (v - u_{sr})f_s + v_{t,sr}^2 \nabla_v f_s$ . Integrate (B1) by parts and use the fact that  $f_s \to 0$  faster than any polynomial or logarithmic singularity. In the interest of simplicity we adopt the notation  $\int_{d_v} = \int d^{d_v} v$ , then the time rate of change  $\dot{S}$  becomes

$$\dot{S} = \sum_{s} \int_{d_{v}} \nu_{sr} J_{sr} \nabla_{v} (\ln f_{s} + 1)$$

$$= \sum_{s} \int_{d_{v}} \nu_{sr} \left[ (\boldsymbol{v} - \boldsymbol{u}_{sr}) f_{s} + v_{t,sr}^{2} \nabla_{v} f_{s} \right] \cdot \nabla_{v} \ln f_{s},$$

$$= \sum_{s} \int_{d_{v}} \nu_{sr} \left[ (\boldsymbol{v} - \boldsymbol{u}_{sr}) \cdot \nabla_{v} f_{s} + v_{t,sr}^{2} \nabla_{v} f_{s} \cdot \nabla_{v} \ln f_{s} \right]. \tag{B2}$$

The first term can be integrated again so that, upon discarding the surface term, and adopting the notation  $\dot{\mathcal{N}}_{sr} = v_{sr} d_v n_s$  and  $\dot{\mathcal{T}}_{sr} = v_{sr} v_{t,sr}^2$ , one obtains

$$\dot{S} = \sum_{s} \left( -\dot{\mathcal{N}}_{sr} + \dot{\mathcal{T}}_{sr} \int_{d_{v}} \nabla_{v} f_{s} \cdot \nabla_{v} \ln f_{s} \right). \tag{B3}$$

At this point we can ask what is the distribution function that minimizes  $\dot{S}$ . Given a set of primitive moments  $(u_{sr,i}, v_{t,sr},$  and also  $u_{s,i}, v_{t,s})$  and the virtual displacement  $\delta f_s = f_s - f_{s0}$ , the response of the functional in (B3) is

$$\delta \dot{\mathcal{S}} = \sum_{s} \dot{\mathcal{T}}_{sr} \int_{d_{v}} \left[ \delta \left( \frac{1}{f_{s}} \right) |\nabla_{u} f_{s0}|^{2} + \frac{1}{f_{s0}} \delta |\nabla_{u} f_{s}|^{2} \right],$$

$$\approx \sum_{s} \dot{\mathcal{T}}_{sr} \int_{d_{v}} \frac{1}{f_{s0}} \left( -\frac{\delta f_{s}}{f_{s0}} |\nabla_{u} f_{s0}|^{2} + 2\nabla_{u} f_{s0} \cdot \nabla_{v} \delta f_{s} \right),$$

$$= \sum_{s} \dot{\mathcal{T}}_{sr} \int_{d_{v}} \left\{ \frac{1}{f_{s0}} \left( -\frac{\delta f_{s}}{f_{s0}} \right) |\nabla_{u} f_{s0}|^{2} + 2 \left[ \nabla_{v} \cdot \frac{\delta f_{s}}{f_{s0}} \nabla_{u} f_{s0} - \delta f_{s} \nabla_{v} \cdot \frac{1}{f_{s0}} \nabla_{u} f_{s0} \right] \right\}. \quad (B4)$$

The second term vanishes since  $\delta f_s \to \pm \infty$  as  $v_i \to \pm \infty$ . Thus at an extremum

$$\delta \dot{S} = \sum_{s} \dot{T}_{sr} \int_{d_{v}} \left[ -\frac{1}{f_{s0}^{2}} |\nabla_{v} f_{s0}|^{2} - 2\nabla_{v} \cdot \frac{1}{f_{s0}} \nabla_{v} f_{s0} \right] \delta f_{s}$$
 (B5)

must vanish, and since (B3) has no upper bound this extremum must be a minimum. At this point we can impose the conditions

$$\int_{d_v} \delta f_s = 0, \tag{B6}$$

$$\int_{d_v} m_s \mathbf{v} \, \delta f_s = 0, \tag{B7}$$

$$\int_{d_v} \frac{1}{2} m_s v^2 \, \delta f_s = 0,\tag{B8}$$

requiring the virtual displacement to not alter the moments of the solution (but does not mean that the moments are constant in time). From (B5)–(B8) we can deduce that for (B5) to vanish for all displacements  $\delta f_s$  it must be that

$$|\nabla_{\mathbf{v}} \ln f_{s0}|^2 + 2\nabla_{\mathbf{v}}^2 \ln f_{s0} = a + \mathbf{b} \cdot \mathbf{v} + cv^2,$$
(B9)

where a, b and c are constants. We can re-write this equation as

$$h(t, \mathbf{x}, \mathbf{v})^2 + 2\nabla_{\mathbf{v}} \cdot \mathbf{h}(t, \mathbf{x}, \mathbf{v}) = a + \mathbf{b} \cdot \mathbf{v} + cv^2, \tag{B10}$$

where  $h(t, x, v) = \nabla_v \ln f_{s0}$ . We claim that the solution to this nonlinear inhomogeneous equation is

$$h(t, \mathbf{x}, \mathbf{v}) = h_0 + h_1 \mathbf{v},\tag{B11}$$

with  $h_0$  and  $h_1$  yet undetermined constants. Check by substituting (B11) into (B10):

$$h(t, \mathbf{x}, \mathbf{v})^2 + 2\nabla_{\mathbf{v}} \cdot h(t, \mathbf{x}, \mathbf{v}) = h_0^2 + 2h_1 h_0 \cdot \mathbf{v} + h_1^2 v^2 + 2\nabla_{\mathbf{v}} \cdot (h_0 + h_1 \mathbf{v}),$$
(B12)

which has the same form as the right-hand side of (B10) with  $a = h_0^2 + 2d_v h_1$ ,  $b = 2h_1 h_0$  and  $c = h_1^2$ . Going back to the definition of  $h(t, x_i, v_i)$ , we can arrive at

$$\ln f_{s0} = g_0 + \mathbf{h_0} \cdot \mathbf{v} + \frac{1}{2}h_1v^2, 
\Rightarrow f_{s0} = A \exp\left(\mathbf{h_0} \cdot \mathbf{v} + \frac{1}{2}h_1v^2\right).$$
(B13)

We can now explore whether our minimized  $\dot{S}$  falls below zero. For this we rewrite (B3) making use of vanishing total derivatives

$$\min\left(\dot{\mathcal{S}}\right) = \sum_{s} \left(-\dot{\mathcal{N}}_{sr} - \dot{\mathcal{T}}_{sr} \int_{d_v} f_{s0} \nabla_v \cdot \frac{1}{f_{s0}} \nabla_v f_{s0}\right),\tag{B14}$$

and, from (B9),

$$f_{s0}\nabla_{\mathbf{v}} \cdot \frac{1}{f_{s0}}\nabla_{\mathbf{v}}f_{s0} = \frac{a + \mathbf{b} \cdot \mathbf{v} + cv^2}{2}f_{s0} - \frac{1}{2f_{s0}}|\nabla_{\mathbf{v}}f_{s0}|^2.$$
 (B15)

Putting these two equations together we have

$$\min\left(\dot{\mathcal{S}}\right) = \sum_{s} \left[ -\dot{\mathcal{N}}_{sr} - \frac{1}{2}\dot{\mathcal{T}}_{sr} \int_{d_v} \left( a + \boldsymbol{b} \cdot \boldsymbol{v} + cv^2 - |\nabla_v \ln f_{s0}|^2 \right) f_{s0} \right]. \tag{B16}$$

Take the derivative of (B13) and insert it into (B16) to obtain

$$\min\left(\dot{\mathcal{S}}\right) = \sum_{s} \left[ -\dot{\mathcal{N}}_{sr} - \frac{1}{2}\dot{\mathcal{T}}_{sr} \int_{d_v} \left( a + \boldsymbol{b} \cdot \boldsymbol{v} + cv^2 - |\boldsymbol{h_0} + h_1 \boldsymbol{v}|^2 \right) f_{s0} \right]. \tag{B17}$$

Employing the definitions of a,  $b_i$  and c above this becomes

$$\min\left(\dot{\mathcal{S}}\right) = \sum_{s} \left(-\dot{\mathcal{N}}_{sr} - d_v h_1 \dot{\mathcal{T}}_{sr} \int_{d_v} f_{s0}\right). \tag{B18}$$

If we require that the zeroth moment of  $f_{s0}$  equals  $n_s$ , we find that

$$f_{s0} = n_s \left( -\frac{h_1}{2\pi} \right)^{d_v/2} \exp\left[ \frac{(h_0 + h_1 v)^2}{2h_1} \right].$$
 (B19)

Identify  $h_1$  with  $-v_{t,s}^{-2}$  such that the minimizing function becomes

$$f_{s0} = \frac{n_s}{\left(2\pi v_{t,s}^2\right)^{d_v/2}} \exp\left[-\frac{\left(v_{t,s}^2 \mathbf{h_0} - \mathbf{v}\right)^2}{2v_{t,s}^2}\right],\tag{B20}$$

and by taking the first moment of this distribution it would become clear that  $v_{t,s}^2 h_0 = u_s$ . The minimizing distribution is thus a Maxwellian with number density  $n_s$ , mean flow velocity  $u_s$  and thermal speed  $v_{t,s}$ . Since we have found a single distribution that minimizes  $\dot{S}$  then the minimum given below must be global.

One can show that if the two colliding distributions are Maxwellian, that the total entropy does not decrease. We can check this here by going back to (B18), and find that the minimum entropy rate of change is

$$\min\left(\dot{\mathcal{S}}\right) = -d_v \sum_{s} n_s \nu_{sr} \left(1 - \frac{v_{t,sr}^2}{v_{t,s}^2}\right). \tag{B21}$$

At this point one must substitute the definition for the cross-species thermal speed in (2.9) to yield

$$\min(\dot{S}) = d_v \sum_{s} \frac{n_s v_{sr}}{v_{t,s}^2} \frac{\delta_s}{2} \frac{1+\beta}{1+\frac{m_r}{m_s}} \left[ \frac{m_r}{m_s} v_{t,r}^2 + \frac{1}{d_v} \frac{m_r}{m_s} (\boldsymbol{u}_s - \boldsymbol{u}_r)^2 - v_{t,s}^2 \right],$$

$$= d_v \frac{m_s n_s v_{sr}}{v_{t,s}^2} \frac{\delta_s}{2} \frac{1+\beta}{m_s + m_r} \sum_{s} \left[ \frac{T_r}{T_s} + \frac{1}{d_v} \frac{m_r}{m_s} \frac{(\boldsymbol{u}_s - \boldsymbol{u}_r)^2}{v_{t,s}^2} - 1 \right],$$

$$= d_v \frac{m_s n_s v_{sr}}{v_{t,s}^2} \frac{\delta_s}{2} \frac{1+\beta}{m_s + m_r} \left[ \frac{(T_r - T_s)^2}{T_s T_r} + \frac{1}{d_v} \left( \frac{m_r}{m_s} \frac{1}{v_{t,s}^2} + \frac{m_s}{m_r} \frac{1}{v_{t,r}^2} \right) (\boldsymbol{u}_s - \boldsymbol{u}_r)^2 \right] \geqslant 0,$$
(B22)

and thus the entropy cannot decrease and the *H*-theorem of this nonlinear full-*f* multispecies collision model is guaranteed.

# Appendix C. Energy conservation with piecewise-linear basis

C.1. Cartesian p = 1 energy conservation

The derivation of a constraint on the operator to conserve energy in § 3.2 relied on  $v^2$  belonging to the space span by the basis set. For piecewise-linear basis (p=1) that is not the case, so instead we can guarantee that the algorithm preserves the projection of the energy onto the basis. We use the notation and strategy first outlined in Hakim *et al.* (2020) for self-species collisions;  $\overline{v^2}$  is the projection of  $v^2$  onto the basis. For the energy to be conserved the left-hand side of (3.1) has to be zero after making the substitution  $\psi_{\ell} = m_s \overline{v^2}/2$ , summing over species and over all cells. Those steps lead to the relation

$$\sum_{j} \int_{x_{i-1/2}}^{x_{i+1/2}} \left\{ \frac{m_s}{2} v_{sr} \left[ \left( \overline{v^2} G_s - \frac{\partial \overline{v^2}}{\partial v} v_{t,sr}^2 \hat{f}_s \right) \Big|_{v_{j-1/2}}^{v_{j+1/2}} - \int_{v_{j-1/2}}^{v_{j+1/2}} \frac{\partial \overline{v^2}}{\partial v} (v - u_{sr}) f_s \, dv \right] + \frac{m_s}{2} v_{rs} \left[ \left( \overline{v^2} G_r - \frac{\partial \overline{v^2}}{\partial v} v_{t,rs}^2 \hat{f}_r \right) \Big|_{v_{j-1/2}}^{v_{j+1/2}} - \int_{v_{j-1/2}}^{v_{j+1/2}} \frac{\partial \overline{v^2}}{\partial v} (v - u_{rs}) f_r \, dv \right] \right\} dx = 0, \quad (C1)$$

where we used  $\partial^2 \overline{v^2} / \partial v^2 = 0$ . Next, we use the fact that (Hakim *et al.* 2020)

$$\frac{1}{2}\frac{\partial\overline{v^2}}{\partial v} = \check{v}_j = \frac{v_{j-1/2} + v_{j+1/2}}{2} \tag{C2}$$

(the cell centre) and the continuity of  $\overline{v^2}G_s$  as well at the zero flux boundary conditions, to turn (C1) into

$$\int_{x_{i-1/2}}^{x_{i+1/2}} \sum_{j} \left\{ m_{s} v_{sr} \left[ -\check{v}_{j} v_{t,sr}^{2} \hat{f}_{s} \Big|_{v_{j-1/2}}^{v_{j+1/2}} - \int_{v_{j-1/2}}^{v_{j+1/2}} \check{v}_{j} (v - u_{sr}) f_{s} dv \right] + m_{s} v_{rs} \left[ -\check{v}_{j} v_{t,rs}^{2} \hat{f}_{r} \Big|_{v_{j-1/2}}^{v_{j+1/2}} - \int_{v_{j-1/2}}^{v_{j+1/2}} \check{v}_{j} (v - u_{rs}) f_{r} dv \right] \right\} dx = 0.$$
 (C3)

Carrying out the velocity integrals this equation becomes

$$\int_{x_{i-1/2}}^{x_{i+1/2}} \left\{ m_s \nu_{sr} \left[ -v_{t,sr}^2 \left( \check{v}_j f_s(\nu_{j\pm 1/2}) \Big|_{j_{\min}}^{j_{\max}} - M_{0,s}^{\star} \right) - \left( M_{2,s}^{\star} - u_{sr} M_{1,s}^{\star} \right) \right] \right. \\
\left. + m_s \nu_{rs} \left[ -v_{t,rs}^2 \left( \check{v}_j f_r(\nu_{j\pm 1/2}) \Big|_{j_{\min}}^{j_{\max}} - M_{0,r}^{\star} \right) - \left( M_{2,r}^{\star} - u_{rs} M_{1,r}^{\star} \right) \right] \right\} dx = 0, \quad (C4)$$

where the  $\pm$  sign is used when evaluating at  $j_{\text{max}}/j_{\text{min}}$  and we have introduced the star moments

$$M_{0,s}^{\star} = \sum_{j=1}^{N_v - 1} (\check{v}_{j+1} - \check{v}_j) \hat{f}_{s,j+1/2},$$

$$M_{1,s}^{\star} = \sum_{j=1}^{N_v} \int_{v_{j-1/2}}^{v_{j+1/2}} \check{v}_j f_s \, \mathrm{d}v,$$

$$M_{2,s}^{\star} = \sum_{j=1}^{N_v} \int_{v_{j-1/2}}^{v_{j+1/2}} \check{v}_j v f_s \, \mathrm{d}v.$$
(C5)

Therefore, our DG scheme will conserve energy if we enforce the following weak constraint:

$$m_{s}v_{sr}\left[u_{sr}M_{1,s}^{\star}+v_{t,sr}^{2}\left(M_{0,s}^{\star}-\check{v}_{j}f_{s}(v_{j\pm1/2})\Big|_{j_{\min}}^{j_{\max}}\right)\right] + m_{r}v_{rs}\left[u_{rs}M_{1,r}^{\star}+v_{t,rs}^{2}\left(M_{0,r}^{\star}-\check{v}_{j}f_{r}(v_{j\pm1/2})\Big|_{j_{\min}}^{j_{\max}}\right)\right] \doteq m_{s}v_{sr}M_{2,s}^{\star}+m_{r}v_{rs}M_{2,r}^{\star}.$$
 (C6)

In order to formulate an energy-conserving LBO-G with p=1 we also need to re-examine the thermal relaxation rate of the discrete operator, (3.12). If we instead substitute  $\psi_{\ell} = m_s \overline{(v-u_s)^2}/2 = m_s \overline{(v^2-2vu_s+u_s^2)}/2$  into (3.1) and sum over velocity-space cells we get

$$\sum_{j} \int_{K_{i,j}} \frac{m_s}{2} \overline{(v - u_s)^2} \left( \frac{\mathrm{d}f_s}{\mathrm{d}t} \right)_c \, \mathrm{d}x \, \mathrm{d}v = - \int_{x_{i-1/2}}^{x_{i+1/2}} m_s v_{sr} \sum_{j} \left[ \left( \check{v}_j - u_s \right) v_{t,sr}^2 \hat{f}_s \Big|_{v_{j-1/2}}^{v_{j+1/2}} + \int_{v_{j-1/2}}^{v_{j+1/2}} \left( \check{v}_j - u_s \right) (v - u_{sr}) f_s \, \mathrm{d}v \right] \mathrm{d}x, \quad (C7)$$

having used the continuity of  $\overline{(v-u_s)^2}G_s$ , its boundary conditions, (C2) and  $\partial^2 \overline{v^2}/\partial v^2 = 0$ . Carry out the velocity-space integrals on the right as well as the sum over j in order to land at

$$\sum_{j} \int_{K_{i,j}} \frac{m_{s}}{2} \overline{(v - u_{s})^{2}} \left( \frac{\mathrm{d}f_{s}}{\mathrm{d}t} \right)_{c} dx dv$$

$$= \int_{x_{i-1/2}}^{x_{i+1/2}} m_{s} v_{sr} \left[ v_{t,sr}^{2} \left( M_{0,s}^{\star} - \check{v}_{j} f_{s} (v_{j\pm 1/2}) \Big|_{j_{\min}}^{j_{\max}} + u_{s} \hat{f}_{s} \Big|_{v_{j_{\min}-1/2}}^{v_{j_{\max}+1/2}} \right) + u_{sr} \left( M_{1,s}^{\star} - u_{s} M_{0,s} \right) - \left( M_{2,s}^{\star} - u_{s} M_{1,s} \right) \right] dx. \tag{C8}$$

Therefore, when using p = 1 bases we enforce the equality of the relaxation rates with

$$m_{s}v_{sr}\left[u_{sr}\left(M_{1,s}^{\star}-u_{s}M_{0,s}\right)+v_{t,sr}^{2}\left(M_{0,s}^{\star}-\check{v}_{j}f_{s}(v_{j\pm1/2})\Big|_{j_{\min}}^{j_{\max}}+u_{s}\hat{f}_{s}\Big|_{v_{j_{\min}-1/2}}^{v_{j_{\max}+1/2}}\right)\right.$$

$$\left.-m_{r}v_{rs}\left[u_{rs}\left(M_{1,r}^{\star}-u_{r}M_{0,r}\right)+v_{t,rs}^{2}\left(M_{0,r}^{\star}-\check{v}_{j}f_{r}(v_{j\pm1/2})\Big|_{j_{\min}}^{j_{\max}}+u_{r}\hat{f}_{r}\Big|_{v_{j_{\min}-1/2}}^{v_{j_{\max}+1/2}}\right)\right]$$

$$\doteq m_{s}v_{sr}\left(M_{2,s}^{\star}-u_{s}M_{1,s}\right)-m_{r}v_{rs}\left(M_{2,r}^{\star}-u_{r}M_{1,r}\right)$$

$$+\frac{\alpha_{E}}{M_{0,s}M_{0,r}}\left[m_{r}M_{0,s}\left(M_{2,r}-u_{r,i}M_{1i,r}\right)-m_{s}M_{0,r}\left(M_{2,s}-u_{s,i}M_{1i,s}\right)\right]$$

$$+\frac{m_{r}-m_{s}}{2}\left(u_{s,i}-u_{r,i}\right)\left(M_{0,r}M_{1i,s}-M_{0,s}M_{1i,r}\right)\right]. \tag{C9}$$

C.2. Gyroaveraged p = 1 energy conservation

Energy conservation with p = 1 basis functions is also possible with the gyroaveraged operator in (2.35). The discretization and calculation of the cross-primitive moments

follows in the vein of that explained in § 3.4.1, although this time we must consider the projection of the  $v_{\parallel}^2$  onto the p=1 as was done for the non-gyroaveraged operator in the previous section. Substituting  $\psi_{\ell} = m_s \overline{v_{\parallel}^2}/2$  into the weak form of the gyroaveraged collision operator, summing over velocity-space cells and species we obtain the following constraint:

$$\begin{split} m_{s}v_{sr} \left\{ u_{\parallel s}rM_{1\parallel,s}^{\star} + v_{t,sr}^{2} \left[ M_{0,s}^{\star} + 2M_{0,s} - \frac{2\pi}{m_{s}} \left( \int \check{v}_{\parallel j} f_{s}(v_{\parallel j\pm 1/2}) \right|_{j_{\min}}^{j_{\max}} \mathrm{d}\mu \right. \\ \left. + 2 \int \mu f_{s} \Big|_{\mu_{\min}}^{\mu_{\max}} \mathrm{d}v_{\parallel} \right) \right] \right\} \\ \left. + m_{r}v_{rs} \left\{ u_{rs}M_{1\parallel,r}^{\star} + v_{t,rs}^{2} \left[ M_{0,r}^{\star} + 2M_{0,r} - \frac{2\pi}{m_{r}} \left( \int \check{v}_{\parallel j} f_{r}(v_{\parallel j\pm 1/2}) \Big|_{j_{\min}}^{j_{\max}} \mathrm{d}\mu \right. \right. \\ \left. + 2 \int \mu f_{r} \Big|_{\mu_{\min}}^{\mu_{\max}} \mathrm{d}v_{\parallel} \right) \right] \right\} \doteq m_{s}v_{sr}M_{2,s}^{\star} + m_{r}v_{rs}M_{2,r}^{\star}. \end{split}$$
 (C10)

In addition to energy conservation the gyroaveraged LBO-G requires the discrete thermal relaxation rate of the operator, which we must re-calculate assuming p=1 basis functions. Multiplying the discrete gyroaveraged LBO by  $\psi_\ell = m_s (v-u_{\parallel s})^2/2 + \mu B$ , integrating over phase space and summing over velocity-space cells we obtain the following discrete relaxation rate:

$$\begin{split} & \sum_{j,k} \int_{K_{i,j,k}} \left[ \frac{m_s}{2} \overline{\left( v_{\parallel} - u_{\parallel s} \right)^2} + \mu B \right] \left( \frac{\partial f_s}{\partial t} \right)_c \, \mathrm{d}x \, \mathrm{d}v_{\parallel} \, \mathrm{d}\mu \\ & = v_{sr} \sum_{j,k} \left( \int_{\mu_{k-1/2}}^{\mu_{k+1/2}} \left\{ \left[ \frac{m_s}{2} \overline{\left( v_{\parallel} - u_{\parallel s} \right)^2} + \mu B \right] G_{v_{\parallel}s} - m_s \left( \check{v}_{\parallel j} - u_{\parallel s} \right) v_{t,sr}^2 \hat{f}_s \right\} \Big|_{v_{\parallel j-1/2}}^{v_{\parallel j+1/2}} \, \mathrm{d}\mu \\ & + \int_{v_{\parallel j-1/2}}^{v_{\parallel j+1/2}} \left\{ \left[ \frac{m_s}{2} \overline{\left( v_{\parallel} - u_{\parallel s} \right)^2} + \mu B \right] G_{\mu s} - 2\mu m_s v_{t,sr}^2 \hat{f}_s \right\} \Big|_{\mu_{k-1/2}}^{\mu_{k+1/2}} \, \mathrm{d}v_{\parallel} \\ & - \int_{K_{i,i,k}} \left[ m_s \left( \check{v}_{\parallel j} - u_{\parallel s} \right) \left( v_{\parallel} - u_{\parallel sr} \right) f_s + B2\mu f_s - 2m_s v_{t,sr}^2 f_s \right] \, \mathrm{d}x \, \mathrm{d}v_{\parallel} \, \mathrm{d}\mu \right), \end{split}$$
 (C11)

where j(k) labels the cell along  $v_{\parallel}(\mu)$ , and we used the fact that  $m_s(v-u_{\parallel s})^2/2 + \mu B$  is linear in  $v_{\parallel}$  and that its  $v_{\parallel}$  derivative is  $m_s(\check{v}_{\parallel j}-u_{\parallel s})$ . In (C11) the  $G_{v_{\parallel s}}$  and  $G_{\mu s}$  are numerical fluxes (Francisquez *et al.* 2020). Doing the velocity-space integrals, carrying out the sums over velocity-space cells, using the continuity of  $G_{v_{\parallel s}}$ ,  $G_{\mu s}$  and  $\hat{f}_s$  and the zero-flux boundary conditions (BCs) one obtains

$$\sum_{i,k} \int_{K_{l,i,k}} \left[ \frac{m_s}{2} \overline{\left(v_{\parallel} - u_{\parallel s}\right)^2} + \mu B \right] \left( \frac{\partial f_s}{\partial t} \right)_c dx dv_{\parallel} d\mu$$

$$= m_{s} v_{sr} \int_{x_{i-1/2}}^{x_{i+1/2}} \left\{ v_{t,sr}^{2} \left[ 2M_{0,s} + M_{0,s}^{\star} - \frac{2\pi}{m_{s}} \left( \sum_{k} \int_{\mu_{k-1/2}}^{\mu_{k+1/2}} \check{v}_{\parallel j} f_{s}(v_{\parallel j\pm 1/2}) \right|_{j_{\min}}^{j_{\max}} d\mu \right. \\ \left. + 2 \sum_{j} \int_{v_{\parallel j-1/2}}^{v_{\parallel j+1/2}} \mu f_{s} \Big|_{\mu_{\min}}^{\mu_{\max}} dv_{\parallel} \right) \right] + u_{\parallel sr} \left( M_{1\parallel,s}^{\star} - u_{\parallel s} M_{0,s} \right) - \left( M_{2,s}^{\star} - u_{\parallel s} M_{1\parallel,s} \right) \right\} dx.$$
(C12)

Using this equation we can enforce the equality between the discrete thermal relaxation rates via

$$\begin{split} m_{s}v_{sr} \left\{ u_{\parallel sr} \left( M_{1\parallel,s}^{\star} - u_{\parallel s} M_{0,s} \right) + v_{t,sr}^{2} \left[ 2M_{0,s} + M_{0,s}^{\star} \right. \right. \\ &\left. - \frac{2\pi}{m_{s}} \left( \sum_{k} \int_{\mu_{k-1/2}}^{\mu_{k+1/2}} \check{v}_{\parallel j} f_{s} (v_{\parallel j\pm 1/2}) \Big|_{j_{\min}}^{j_{\max}} d\mu + 2 \sum_{j} \int_{v_{\parallel j-1/2}}^{v_{\parallel j+1/2}} \mu f_{s} \Big|_{\mu_{\min}}^{\mu_{\max}} dv_{\parallel} \right) \right] \right\} \\ &\left. - m_{r} v_{rs} \left\{ u_{\parallel rs} \left( M_{1\parallel,r}^{\star} - u_{\parallel r} M_{0,r} \right) + v_{t,rs}^{2} \left[ 2M_{0,r} + M_{0,r}^{\star} \right. \right. \right. \\ &\left. - \frac{2\pi}{m_{r}} \left( \sum_{k} \int_{\mu_{k-1/2}}^{\mu_{k+1/2}} \check{v}_{\parallel j} f_{r} (v_{\parallel j\pm 1/2}) \Big|_{j_{\min}}^{j_{\max}} d\mu + 2 \sum_{j} \int_{v_{\parallel j-1/2}}^{v_{\parallel j+1/2}} \mu f_{r} \Big|_{\mu_{\min}}^{\mu_{\max}} dv_{\parallel} \right) \right] \right\} \\ & \doteq m_{s} v_{sr} \left( M_{2,s}^{\star} - u_{\parallel s} M_{1\parallel,s} \right) - m_{r} v_{rs} \left( M_{2,r}^{\star} - u_{\parallel r} M_{1\parallel,r} \right) \\ &\left. + \frac{\alpha_{E}}{M_{0,s} M_{0,r}} \left[ m_{r} M_{0,s} \left( M_{2,r} - u_{\parallel r} M_{1\parallel,r} \right) - m_{s} M_{0,r} \left( M_{2,s} - u_{\parallel s} M_{1\parallel,s} \right) \right. \\ &\left. + \frac{m_{r} - m_{s}}{2} \left( u_{\parallel s} - u_{\parallel r} \right) \left( M_{0,r} M_{1\parallel,s} - M_{0,s} M_{1\parallel,r} \right) \right]. \end{split}$$
 (C13)

#### REFERENCES

- ABEL, I.G., BARNES, M., COWLEY, S.C., DORLAND, W. & SCHEKOCHIHIN, A.A. 2008 Linearized model Fokker–Planck collision operators for gyrokinetic simulations. I. Theory. *Phys. Plasmas* 15 (12), 122509.
- ANDERSON, M.W. & O'NEIL, T.M. 2007 Eigenfunctions and eigenvalues of the Dougherty collision operator. *Phys. Plasmas* **14** (5), 052103.
- BHATNAGAR, P.L., GROSS, E.P. & KROOK, M. 1954 A model for collision processes in gases. I. Small amplitude processes in charged and neutral one-component systems. *Phys. Rev.* **94**, 511–525.
- COCKBURN, B. & SHU, C.-W. 1998 The local discontinuous Galerkin method for time-dependent convection-diffusion systems. SIAM J. Numer. Anal. 35 (6), 2440–2463.
- DOUGHERTY, J.P. 1964 Model Fokker–Planck equation for a plasma and its solution. *Phys. Fluids* **7** (11), 1788–1799.
- DOUGHERTY, J.P. & WATSON, S.R. 1967 Model Fokker–Planck equations: Part 2. The equation for a multicomponent plasma. *J. Plasma Phys.* 1 (3), 317–326.
- ESTÈVE, D., GARBET, X., SARAZIN, Y., GRANDGIRARD, V., CARTIER-MICHAUD, T., DIF-PRADALIER, G., GHENDRIH, P., LATU, G. & NORSCINI, C. 2015 A multi-species collisional operator for full-F gyrokinetics. *Phys. Plasmas* 22 (12), 122506.
- Francisquez, M., Bernard, T.N., Mandell, N.R., Hammett, G.W. & Hakim, A. 2020 Conservative discontinuous Galerkin scheme of a gyro-averaged Dougherty collision operator. *Nucl. Fusion* **60** (9), 096021.

- FREI, B.J., BALL, J., HOFFMANN, A.C.D., JORGE, R., RICCI, P. & STENGER, L. 2021 Development of advanced linearized gyrokinetic collision operators using a moment approach. *J. Plasma Phys.* 87, 905870501.
- GKEYLL 2020 The Gkeyll 2.0 Code: documentation home. http://gkeyll.readthedocs.io.
- GREENE, J.M. 1973 Improved Bhatnagar–Gross–Krook model of electron-ion collisions. *Phys. Fluids* **16** (11), 2022–2023.
- HAACK, J.R., HAUCK, C.D. & MURILLO, M.S. 2017 A conservative, entropic multispecies BGK model. *J. Stat. Phys.* 168 (4), 826–856.
- HAGER, R., YOON, E.S., KU, S., D'AZEVEDO, E.F., WORLEY, P.H. & CHANG, C.S. 2016 A fully non-linear multi-species Fokker–Planck–Landau collision operator for simulation of fusion plasma. *J. Comput. Phys.* 315, 644–660.
- HAKIM, A., FRANCISQUEZ, M., JUNO, J. & HAMMETT, G.W. 2020 Conservative discontinuous Galerkin schemes for nonlinear Dougherty–Fokker–Planck collision operators. J. Plasma Phys. 86 (4), 905860403.
- HAKIM, A. & JUNO, J. 2020 Alias-free, matrix-free, and quadrature-free discontinuous Galerkin algorithms for (plasma) kinetic equations. In *Proceedings of the International Conference for High Performance Computing, Networking, Storage and Analysis, SC '20*, vol. 73. IEEE.
- HESTHAVEN, J.S. & WARBURTON, T. 2007 Nodal Discontinuous Galerkin Methods: Algorithms, Analysis, and Applications. Springer.
- HINTON, F.L. & HAZELTINE, R.D. 1976 Theory of plasma transport in toroidal confinement systems. *Rev. Mod. Phys.* **48**, 239–308.
- HIRVIJOKI, E., BRIZARD, A.J. & PFEFFERLÉ, D. 2017 Differential formulation of the gyrokinetic Landau operator. *J. Plasma Phys.* **83** (1), 595830102.
- HUBA, J.D. 2013 NRL Plasma Formulary, Supported by the Office of Naval Research. Naval Research Laboratory.
- JORGE, R., RICCI, P., BRUNNER, S., GAMBA, S., KONOVETS, V., LOUREIRO, N.F., PERRONE, L.M. & TEIXEIRA, N. 2019 Linear theory of electron-plasma waves at arbitrary collisionality. *J. Plasma Phys.* **85** (2), 905850211.
- JORGE, R., RICCI, P. & LOUREIRO, N.F. 2018 Theory of the drift-wave instability at arbitrary collisionality. *Phys. Rev. Lett.* **121**, 165001.
- JUNO, J., HAKIM, A., TENBARGE, J., SHI, E. & DORLAND, W. 2018 Discontinuous Galerkin algorithms for fully kinetic plasmas. *J. Comput. Phys.* **353**, 110–147.
- KOLESNIKOV, R.A., WANG, W.X. & HINTON, F.L. 2010 Unlike-particle collision operator for gyrokinetic particle simulations. *J. Comput. Phys.* **229** (15), 5564–5572.
- VAN LEER, B. & LO, M. 2007 A discontinuous Galerkin method for diffusion based on recovery. In *18th AIAA Computational Fluid Dynamics Conference*, *AIAA* 2007-4083, pp. 1–12. American Institute of Aeronautics.
- VAN LEER, B. & NOMURA, S. 2005 Discontinuous Galerkin for diffusion. In *17th AIAA Computational Fluid Dynamics Conference*, AIAA 2005-5109, pp. 1–30. American Institute of Aeronautics.
- LI, B. & ERNST, D.R. 2011 Gyrokinetic Fokker–Planck collision operator. Phys. Rev. Lett. 106 (19), 195002.
- MANDELL, N.R., HAKIM, A., HAMMETT, G.W. & FRANCISQUEZ, M. 2020 Electromagnetic full-f gyrokinetics in the tokamak edge with discontinuous Galerkin methods. *J. Plasma Phys.* 86, 905860109. arXiv:1908.05653
- MORSE, T.F. 1963 Energy and momentum exchange between nonequipartition gases. *Phys. Fluids* 6 (10), 1420–1427.
- MORSE, T.F. 1964 Kinetic model equations for a gas mixture. Phys. Fluids 7 (12), 2012–2013.
- ONG, R.S.B. & YU, M.Y. 1970 The effect of velocity space diffusion on the universal instability in a plasma. *J. Plasma Phys.* **4** (4), 729–738.
- ONG, R.S.B. & YU, M.Y. 1973 The effect of temperature perturbations on ion-acoustic and drift waves in a weakly collisional plasma. *Plasma Phys.* **15** (7), 659–668.
- PAN, Q. & ERNST, D.R. 2019 Gyrokinetic Landau collision operator in conservative form. *Phys. Rev.* E **99**, 023201.

- PAN, Q., ERNST, D.R. & CRANDALL, P. 2020 First implementation of gyrokinetic exact linearized Landau collision operator and comparison with models. *Phys. Plasmas* 27, 042307.
- PAN, Q., ERNST, D.R. & HATCH, D. 2021 Importance of gyrokinetic exact Fokker–Planck collisions in fusion plasma turbulence. *Phys. Rev.* E **103**, L051202.
- PAN, Q., TOLD, D., SHI, E.L., HAMMETT, G.W. & JENKO, F. 2018 Full-f version of GENE for turbulence in open-field-line systems. *Phys. Plasmas* 25 (6), 062303.
- PEZZI, O., VALENTINI, F. & VELTRI, P. 2015 Collisional relaxation: Landau versus Dougherty operator. *J. Plasma Phys.* 81 (1), 305810107.
- Pusztai, I., Juno, J., Brandenburg, A., Tenbarge, J.M., Hakim, A., Francisquez, M. & Sundström, A. 2020 Dynamo in weakly collisional nonmagnetized plasmas impeded by Landau damping of magnetic fields. *Phys. Rev. Lett.* **124**, 255102.
- ROSENBLUTH, M.N., MACDONALD, W.M. & JUDD, D.L. 1957 Fokker–Planck equation for an inverse-square force. *Phys. Rev.* 107 (1), 1–6.
- SHI, E.L., HAMMETT, G.W., STOLTZFUS-DUECK, T. & HAKIM, A. 2019 Full-f gyrokinetic simulation of turbulence in a helical open-field-line plasma. *Phys. Plasmas* **26** (1), 012307.
- SUGAMA, H., MATSUOKA, S., SATAKE, S., NUNAMI, M. & WATANABE, T.-H. 2019 Improved linearized model collision operator for the highly collisional regime. *Phys. Plasmas* 26 (10), 102108.
- SUGAMA, H., WATANABE, T.-H. & NUNAMI, M. 2009 Linearized model collision operators for multiple ion species plasmas and gyrokinetic entropy balance equations. *Phys. Plasmas* **16** (11), 112503.
- ULBL, P., MICHELS, D. & JENKO, F. 2021 Implementation and verification of a conservative, multi-species, gyro-averaged, full-f, Lenard–Bernstein/Dougherty collision operator in the gyrokinetic code GENE-X. *Contrib. Plasma Phys.* e202100180.